ChemPubSoc
Europe

DOI: 10.1002/chem.201903413

CHEMISTRY
A European Journal
Full Paper

Conjugated Materials

Twisting the TAPPs: *Bay*-Substituted Non-planar Tetraazaperopyrenes and their Reduced Anions

Benjamin A. R. Günther,[a] Sebastian Höfener,[b] Ute Zschieschang,[c] Hubert Wadepohl,[a] Hagen Klauk,[c] and Lutz H. Gade*[a]

Abstract: A new synthesis of tetraazaperopyrenes (TAPPs) starting from a halogenated perylene derivative 3,4,9,10-tetrabromo-1,6,7,12-tetrachloroperylene (**1**) gave access to *bay*-substituted TAPPs for the first time. Selective lithiation of the bromine-positions and subsequent addition of tosyl azide led to the formation of the tetraazidotetrachloroperylene (**2**), which was subsequently reduced by addition of sodium borohydride to the corresponding tetraaminotetrachloroperylene (**3**). Oxidation to its semiquinoidal form **4** and subsequent cyclization with acid chlorides gave rise to a series of *bay*-chlorinated TAPPs. Whereas the aromatic core of the previously studied *ortho*-substituted TAPPs was found to be planar, the steric pressure of the two chlorine substituents on each side leads to the twist of the peropyrene core of approximately 30 degrees, a structural feature also observed in other *bay*-substituted perylene derivatives. An experimental and computational analysis reveals that introducing chloride substituents at these positions leads to slightly increased electron affinities (EA) enabling the selective generation and characterization of the reduced mono-anionic radicals and closed shell di-anionic species. These anions were isolated and characterized by UV/Vis spectroscopy and EPR or NMR, respectively. Processing of the *bay*-chlorinated TAPPs in n-channel organic TFTs revealed electron mobilities of 0.001 to 0.003 $cm^2V^{-1}s^{-1}$. These reduced electron mobilities compared to the *ortho*-halogenated TAPPs are thought to be rooted in the less densely packed solid-state structures.

Introduction

Perylene tetracarboxydiimides (PDIs) have been extensively studied as functional dyes and electronic materials.[1–17] Their properties may be varied widely by substitution at the perylene core and at the imido-N position. The carboxy substituents at the central perylene core render these materials electron acceptors, and this property in particular has been underlying their application in organic electronics.

Different synthetic approaches have been established to functionalize the *bay*-[2,10,18–23] or *ortho*-[24–31] positions selectively or even to fully substitute[26,32,33] the perylene core in a single-step-reaction (Figure 1).[34,35]

A class of molecular dyes which has displayed photophysical and redox properties similar to the ubiquitous PDIs are the tetraazaperopyrenes (TAPPs) which have been investigated for more than a decade.[36–48] Whereas the electron accepting character of the PDIs is due to carboximide substituents at both ends of the perylene core, TAPPs contain two pyrimidine rings fused with the central perylene unit. The electron accepting character of the resulting N-heteropolycycles is thus effectively built into the aromatic core itself rather than substituent-induced. Viewed alternatively, the fourfold isosteric [CH→N] substitution in the parent hydrocarbon peropyrene radically changes its electronic properties while leaving its molecular shape practically unchanged.

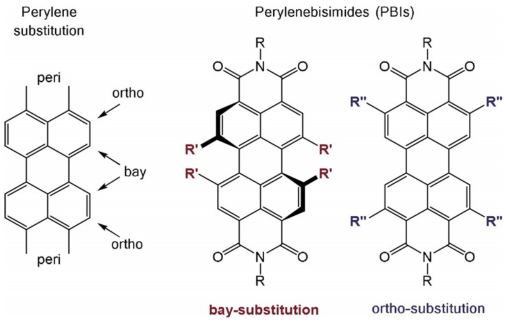

Figure 1. Left: Substituent positions in perylene derivatives. Right: *bay*- and *ortho* substitution in PDIs.

Whereas electrophilic substitution of PDIs and related compounds occurs in the *bay*-positions, the corresponding derivatization of the parent TAPP compounds (**I**) happened exclusively

---

[a] B. A. R. Günther, Prof. Dr. H. Wadepohl, Prof. Dr. L. H. Gade
Anorganisch-Chemisches-Institut, Universität Heidelberg
Im Neuenheimer Feld 270, 69120 Heidelberg (Germany)
E-mail: lutz.gade@uni-heidelberg.de

[b] Dr. S. Höfener
Institute of Physical Chemistry
Karlsruhe Institute of Technology (KIT) P.O. Box 6980
76049 Karlsruhe (Germany)

[c] Dr. U. Zschieschang, Dr. H. Klauk
Max Planck Institute for Solid State Research
Heisenbergstr. 1, 70569 Stuttgart (Germany)

Supporting information and the ORCID identification number(s) for the author(s) of this article can be found under: https://doi.org/10.1002/chem.201903413.

in the *ortho*-position, leaving the *bay*-CH units unaffected and thus maintaining the planar structure of the aromatic core (Scheme 1).[42,44] Manifold derivatization of TAPP derivatives in the 2,9-positions, as well as in the *ortho*-position, has led to a detailed understanding of the molecular behavior and its photophysical and electronic properties. On the other hand, it has not yet been possible to functionalize the inner *bay* position of the peropyrene core, in order to establish a link with the well established PDI chemistry and its further development towards more complex polycyclic aromatics. Thus, a fundamental part of TAPP-chemistry has remained unexplored to date.

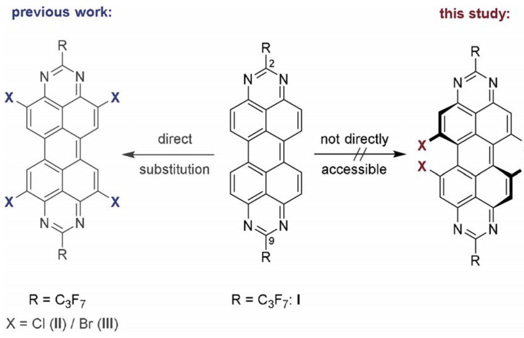

Scheme 1. Approach to synthesize *ortho*-substituted TAPP-derivatives (left, previous work) and inability to functionalize the *bay*-position (right) when starting from earlier parent compound **I**.

In this work, we report a novel TAPP synthesis, which for the first time allowed their *bay* functionalization. Additionally, a detailed study of their reduced species was conducted to gain insights into electronic behavior and their stability. Comparison of the *ortho*- and *bay*-chlorinated TAPPs provided insight into the influence of the different substitution patterns of the peropyrene core.

Results and Discussion

Synthesis of *bay*-chlorinated TAPPs

The starting material for the synthesis of *bay*-substituted TAPPs was tetrabromotetrachloroperylene (**1**), first published in 2014 (Scheme 2).[49] Selective lithiation of the bromine positions and subsequent addition of tosyl azide led to the formation of the tetraazidotetrachloroperylene (**2**), which was subsequently reduced by addition of sodium borohydride to the corresponding tetraaminotetrachloroperylene (**TAP-Cl**, **3**). Analogous to the previously reported non-chlorinated tetraaminoperylene, this compound displayed a tendency to be oxidized under ambient conditions to form the chlorinated diaminoperylenequinone-diimine (**DPDI-Cl**, **4**), however, the reaction proceeded much more slowly than for the parent **DPDI** and occasionally did not go to completion. Therefore, oxidation to the semiquinoidal compound **4** was selectively carried out by the reaction of **3** with activated MnO_2.

By employing the standard ring-closing reaction conditions of the original TAPP-synthesis, the first *bay*-substituted TAPP derivatives with H- or perfluoroalkyl-substituted 2- and 9-position (**5**) were obtained. As opposed to the planar *ortho*-substituted TAPP derivatives, which only possess low solubility in common organic solvents, the twist induced by the *bay*-chlorination leads to a significantly enhanced solubility.

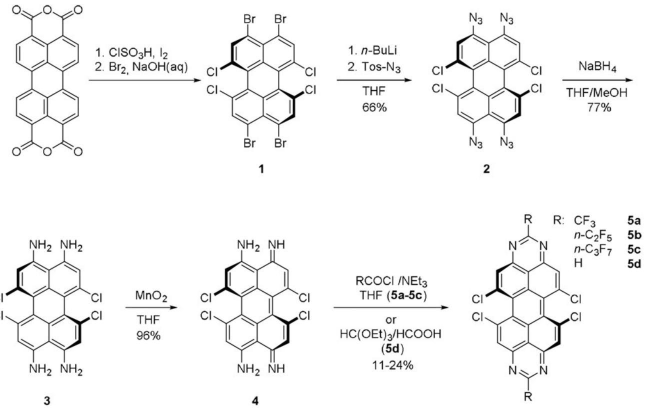

Scheme 2. Synthetic route to the *bay*-chlorinated DPDI analogue (**DPDI-Cl**, **4**) and subsequent ring-closing reaction to the corresponding *bay*-TAPP-Cl **5**.

Crystal structures of 5 a–c

Single crystals of the tetrachlorinated TAPPs **5 a**, **5 b** and **5 c** were grown by slow evaporation of concentrated solutions in chloroform (**5 a** and **5 c**) and toluene (**5 b**) (Figure 2). All three solid-state structures reveal a significant twist between the

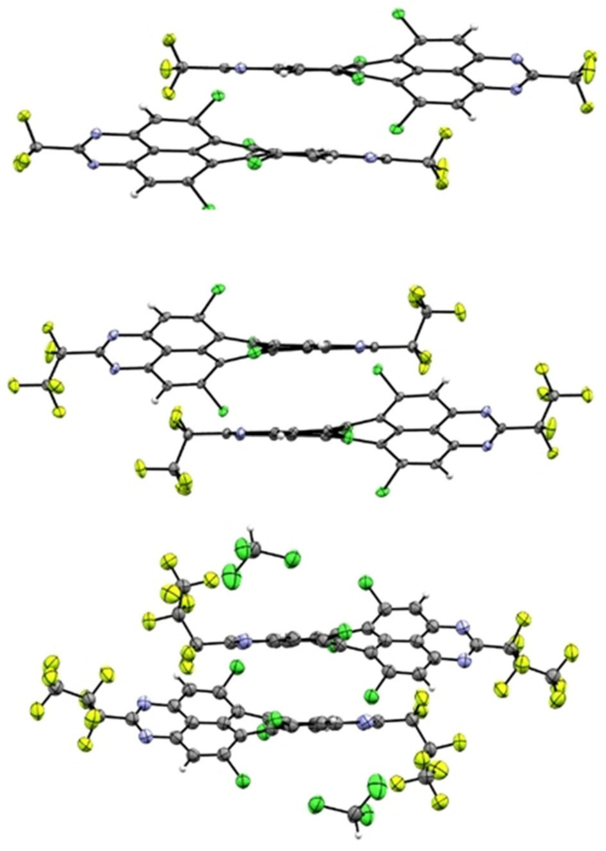

Figure 2. Solid state structure of **5 a** (top), **5 b** (middle) and **5 c** (bottom).

two diazaphenalenyl subunits of the tetraazaperopyrene core: **5 a** (29.4 degrees), **5 b** (30.6 degrees) and **5 c** (32.4 degrees). Whereas the aromatic core of the previously studied *ortho*-substituted TAPPs was found to be planar, the steric pressure of the two chlorine substituents on each side leads to the twist of the peropyrene core, a structural feature also observed in other *bay*-substituted perylene derivatives.[18]

In all three cases, the packing pattern in the solid state is determined by intermolecular stacking of two diazaphenalenyl subunits. This motif leads to distances as close as 3.4 Å between the aromatic core halves of two adjacent molecules, however, the general packing pattern varies for the different perfluorinated alkyl chains (Figure 3). Thus, the CF_3-substituted TAPP **5 a** packs in a zigzag fashion, while the elongation of the fluoroalkyl chains in **5 b** leads to more columnar-like packing pattern. The crystals of **5 c** could not be obtained without co-crystallization of solvent, which renders an assessment of the packing pattern less significant. The key data of the solid-state structures are summarized in Table 1.

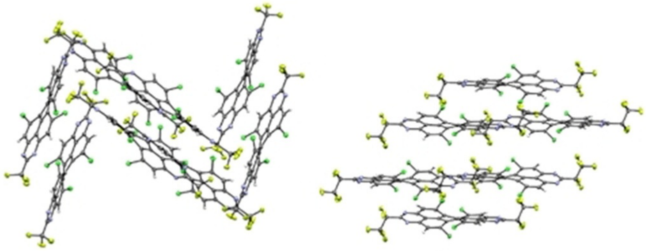

Figure 3. Packing pattern of **5 a** in a zigzag-like fashion (left) and of **5 b** in a columnar pattern (right).

Table 1. Structural parameters of solid-state structures of **5 a**–**c**.

	Crystal system	Space group	π–π Plane distance [Å][a]	Torsion angle [°][b]
5 a	orthorhombic	*Pbca*	3.440	29.43 (0.03)
5 b	monoclinic	*I2/a*	3.535	30.10 (0.03)
5 c	triclinic	$P\bar{1}$	3.603[c]	32.44 (0.07)

[a] π–π Distance was measured between two adjacent diazaphenalenyl-subunits. [b] Torsion angle was measured between both diazaphenalenyl-subunits of one molecule. [c] **5 c** co-crystallized with chloroform, but displaying close packing between pairs of molecules.

Interconversion barrier of atropo-enantiomers

As the steric repulsion between opposing chlorine atoms leads to the aforementioned torsion in the peropyrene backbone, the dye molecules possess helical chirality, leading to *P*- and *M*-atropoisomers (Scheme 3). This helical isomerism has been studied in detail for the structurally similar *bay*-functionalized perylene bisimides,[23,50–58] and the interconversion barrier between the atropo-enantiomers was found to depend on the number and steric demand of the *bay* substituents. Whereas for most PDIs interconversion occurs rapidly at room temperature, larger substituents raise the energy barrier over 22.2 kcal mol^{-1}, which is the minimum barrier required for the isolation of the enantiomers at ambient temperature and the usual timescale of product handling. It was therefore of interest to compare analogously substituted PDI- and TAPP-systems in order to obtain insight into the flexibility of the peropyrene core compared to the PDI system.[54,59]

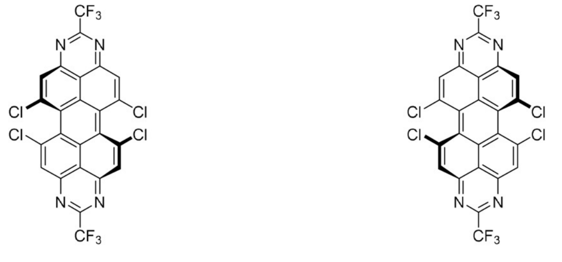

***P*-enantiomer** ***M*-enantiomer**

Scheme 3. The two possible *P*-and *M*-enantiomers of *bay*-substituted TAPPs.

To this end, the interconversion of the atropisomeric *bay*-chlorinated tetraazaperopyrenes, has been modeled theoretically by DFT (Scheme 4). For a potential one-step mechanism involving a planar transition state the energy barrier would be approximately 72 kcal mol^{-1}, thus locking the molecules in a single helical form. As an alternative pathway, the stepwise isomerization was investigated, in which the first transition state is reached via the planarization on only one side of the TAPP, while the opposite side remains in the twisted form. This results in a reduced torsion angle of about 10 degrees compared to 32 degrees in the ground state (Table 2). The computed activation energy was found to be 23.7 kcal mol^{-1}, and the resulting intermediate *bay*-substituted TAPP is characterized by mutually *syn*-oriented chloro substituents. This achiral intermediate is only 9 kcal mol^{-1} higher in energy than the *trans*-oriented conformer and either reacts back to the initial form or to the other atropisomer.

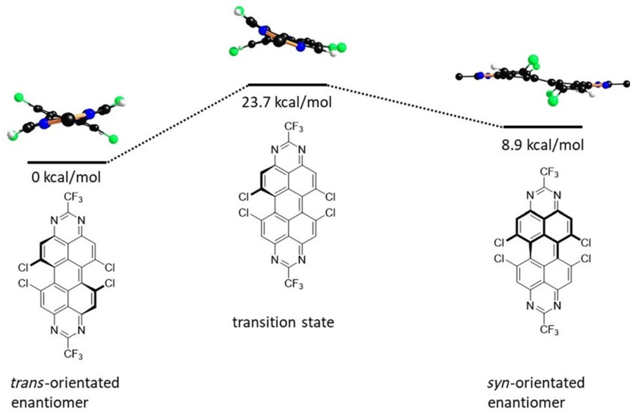

Scheme 4. Calculated relative energies of conversion between atropo-isomers in kcal mol^{-1}.

Table 2. Computed relative energies including the zero-point vibrational energy (ZPVE) and angles of intermediates and the transition state (TS) structure.

	E_{ZPVE} [kcal mol^{-1}]	Torsion angle [°][a]	Imaginary frequency [cm^{-1}]
***trans*-oriented enantiomer**	0	32	
TS	24	10/31	74.96
***syn*-oriented intermediate**	9	23	

[a] Torsion angle was measured using the four C-atoms in the *bay*-area.

This reaction sequence corresponds to the mechanism, Würthner et al. have proposed for the corresponding PDI-systems.[54] Notably, the isomerization barrier of the *bay*-chlorinated TAPPs is very similar to that reported for the PDI-Cl$_4$, which suggests that indeed the PDI-core possesses similar rigidity/flexibilty as the polycyclic aromatic core of the TAPP molecules.

UV/Vis absorption and emission spectra

The UV/Vis absorption and emission spectra of the TAPP derivatives **5a**–**d** recorded in THF are displayed in Figure 4. Similar to the non-twisted *ortho*-substituted TAPP derivatives, the absorption and emission maxima remain unchanged upon variation of the alkyl-substituents in the 2- and 9-positions.[42]

All derivatives were found to exhibit absorption maxima in the range of 468 to 474 nm with vibrational progressions and emission maxima in the range of 496 to 505 nm. As TAPPs are known to aggregate in solution, measurements were repeated in different solvents (DCM and CHCl$_3$) and in different concentrations. However, identical absorption and emission data were observed, leading to the conclusion, that these twisted TAPPs do not tend aggregate in common organic solvents. An overview of the optical properties is given in Table 3.

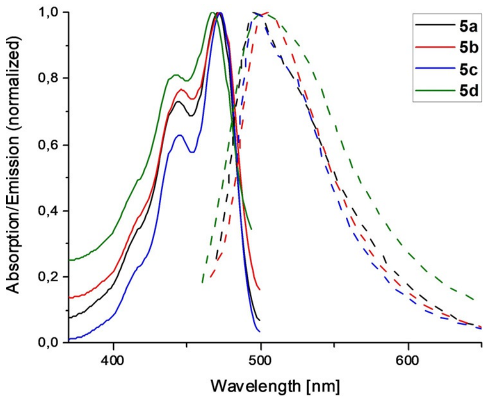

Figure 4. Absorption (continuous line) and emission (dashed line) spectra of *bay*-substituted compounds **5a**–**d** recorded in THF.

Complementing the measurement of the absorption and emission spectra in solution, Table 3 contains vertical transition energies computed at time-dependent density functional theory (TDDFT) level of theory. While the absolute values of the vertical excitation (VE) and the vertical de-excitation (VD) energies deviate from the measured absorption and emission bands by 0.05 and 0.15 eV, respectively, the table confirms that the photophysical data remain unaffected by the variation of substituents in the 2- and 9-positions.

Since computed vertical electronic transition energies cannot be directly related to the experimental results, we also simulated vibrationally resolved adiabatic transitions.[48] Simulated absorption and emission spectra of **5d** are displayed in Figure 5. At zero temperature, the simulated spectra show distinct transitions for individual vibronic transitions.

The spectra do not seem to be dominated by the 0–0 transition and they thus display a Stokes shift of 0.02 eV (140 cm^{-1}) at zero temperature, however, the incorporation of temperature effects leads to a Stokes shift of about 0.07 eV (about 586 cm^{-1}) at 300 K. The finite-temperature spectrum furthermore reproduces the general shape of the experimental spectra as shown in Figure 4, which is characterized by a pronounced vibrational progression at lower wavelength for the absorption but only a broadened band for emission. We note that the experimentally observed Stokes shifts are larger compared to the simulated values, which might be due to solvation effects which are not included in the simulations in vacuum.

Redox properties

To assess the redox chemical properties of the *bay*-chlorinated TAPP derivatives cyclic voltammograms (CVs) of all compounds were recorded. They were found to exhibit two individual and fully reversible one-electron reduction steps to the mono-anionic radical species and the subsequent di-anionic compound. In Figure 6, the CV is shown for compound **5b**.

The energies of the lowest unoccupied molecular orbital (LUMO) were estimated by subtraction of the reversible first reduction potentials obtained from the cyclic voltammograms of

Table 3. Photophysical properties of **5a**–**d** measured in THF and computed vertical electronic excitation (VE) and de-excitation (VD) energies.

	R	λ_{abs} [nm] (log ε)[a]	λ_{em} [nm] (φ_{Em})[a]	0–0 Transition [nm][b]	Stokes shift [cm^{-1}]	λ_{VE} [nm] (DFT)[c]	λ_{VD} [nm] (DFT)[c]
5a	CF$_3$	471 (4.57)	496 (0.12)	482	1070	481	534
5b	C$_2$F$_5$	472 (4.64)	505 (0.09)	485	1384	482	535
5c	C$_3$F$_7$	474 (4.59)	496 (0.10)	484	936	482	536
5d	H	468 (3.98)	501 (0.05)	480	1407	478	532

[a] Absorption and emission spectra were recorded in THF. [b] 0-0-Transition was obtained of the intersection of absorption and emission spectra. [c] Vertical electronic excitation (VE) and de-excitation (VD) energies were calculated using B3LYP as functional and TZVPP as the basis set.

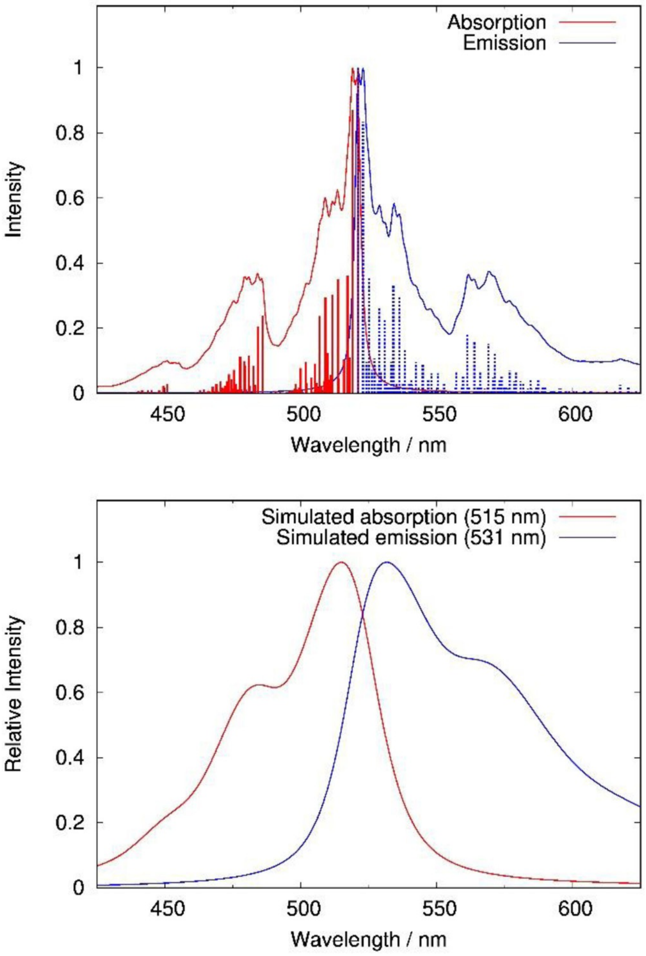

Figure 5. Simulated spectra of compound **5 d** at 0 K (top) and 300 K (bottom), shifted according to the theoretical 0-0 transition energy of 521 nm (2.38 eV), computed in the harmonic approximation at B3LYP/def2-TZVPP level of theory employing D_2 symmetry.

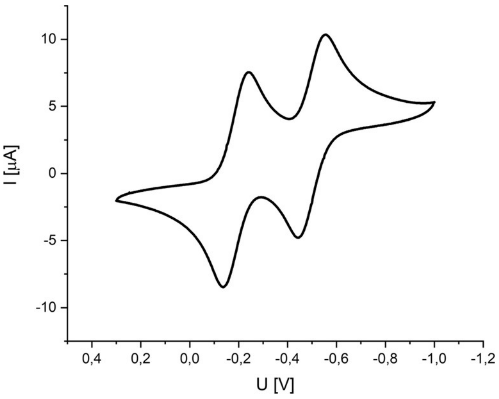

Figure 6. Cyclic Voltammogram of **5 b**, measured in DCM, supp. electrolyte Bu_4NPF_6, reference SCE, sweep rate 50 mV s^{-1}.

the redox potential of ferrocene (4.8 eV for Fc/FC$^+$).[60] As expected, the substituents in the 2- and 9-position have only limited influence on the frontier orbitals, similar to the UV/Vis absorption and emission spectra discussed above. This was backed up by the computational determination of the Kohn–Sham frontier orbital energies determined by DFT.

Whereas the energies of the LUMO and the highest occupied molecular orbital (HOMO) of derivatives **5 a**–**c** are almost identical at around −4.15 eV, the "removal" of the perfluorinated alkyl group leads to an increase of both the HOMO and LUMO energies by about 0.5 eV, resulting in a virtual identical HOMO–LUMO gap of all derivatives. Visualization of the frontier orbitals (Figure 7), reveals the nodal planes of the frontier orbitals along the principal molecular axis in which the substituents in the 2- and 9-positions are located. This also explains the nearly identical absorption and emission spectra of **5 a**–**d** which are dominated by the HOMO–LUMO transition.

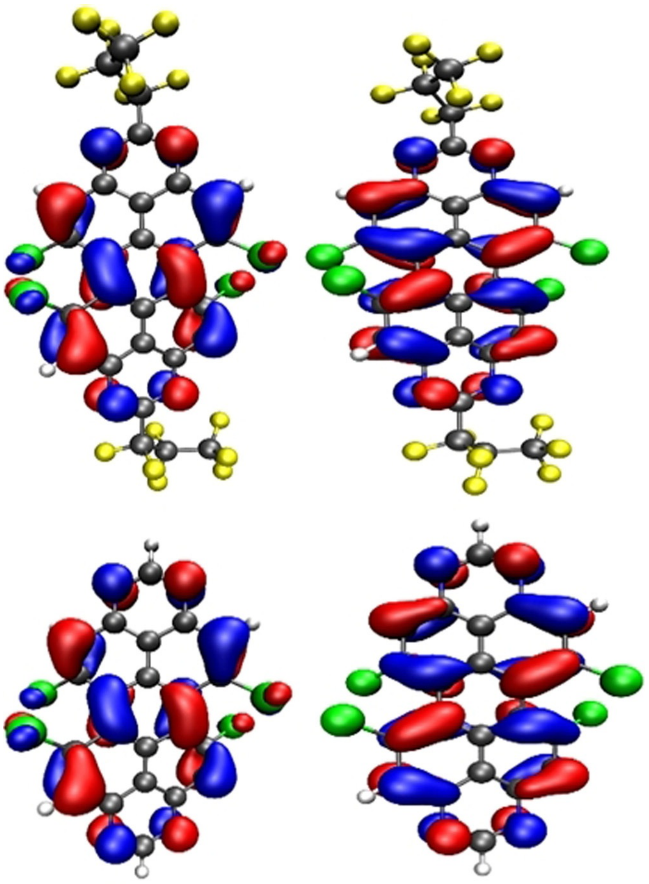

Figure 7. Visualization of the HOMO (left) and LUMO (right) of **5 c** (top) and **5 d** (bottom); level of theory used is B3LYP/def2-SVP, isovalue 0.03.

For the perfluorinated alkyl groups electron affinities between 3.21 and 3.31 eV were found for **5 a**–**c**, whereas the hydrogen-substituted compound **5 d** was found to possess a significantly reduced electron affinity of about 2.73 eV (Table 4). These adiabatic EA values do not differ significantly from vertical EA values obtained from GW methods (The GW method is a way to correct artefacts in Kohn–Sham (KS) methods which employ exchange-correlation (XC) functionals),[61] see Table 2, which indicates that the one-electron reduction does not induce a significant change in the molecular geometry. This corresponds to a small reorganization energy which is desira-

Table 4. Adiabatic electron affinities (aEA) obtained from the ΔSCF approach, vertical electron affinities (vEA) from the GW method, and frontier orbital energies of compounds **5 a**–**d**.

	R	aEA (ΔSCF) [eV][a]	vEA (GW) [eV][a]	$E_{HOMO (DFT)}$ [eV][a]	$E_{HOMO–LUMO}$ [eV]	$E_{LUMO (DFT)}$ [eV][a]	$E_{LUMO (exp, CV)}$ [eV][b]
5 a	CF_3	3.23	3.21	−6.84	2.71	−4.12	−4.14
5 b	C_2F_5	3.22	3.25	−6.86	2.71	−4.15	−4.21
5 c	C_3F_7	3.31	3.27	−6.91	2.71	−4.20	−4.20
5 d	H	2.73	2.75	−6.43	2.72	−3.71	−3.93

[a] Properties were calculated using B3LYP as the functional and a def2-QZVPP as basis set. [b] LUMO energy was estimated from the reversible first reduction potentials obtained from the cyclic voltammograms using the redox potential of ferrocene as reference (4.8 eV for Fc/Fc$^+$).[60]

ble for electron transporting compounds with large λ_+ (reorganization energy for hole transport) and small λ_-(reorganization energy for electron transport).[62]

The two individual one-electron reduction steps occurring consecutively were monitored for **5 a** by UV/Vis spectroscopy in a spectroelectrochemical cell (Figure 8). By applying a potential of −0.5 V the absorption band at 474 nm of the neutral compound completely disappeared, while the formation of a green species with a long-wavelength absorption maximum at 663 nm was detected. This can be attributed to the monoanionic radical TAPP$^{•−}$. The further lowering of the reduction potential to −1.0 V led to the second reduction step, observable by a change of color to purple and the hypsochromic shift of the absorption band to 663 nm. The spectra exhibit relatively well defined isosbestic points at 400 nm and 495 nm, indicating that both reduction steps proceed cleanly and without significant further conversions.

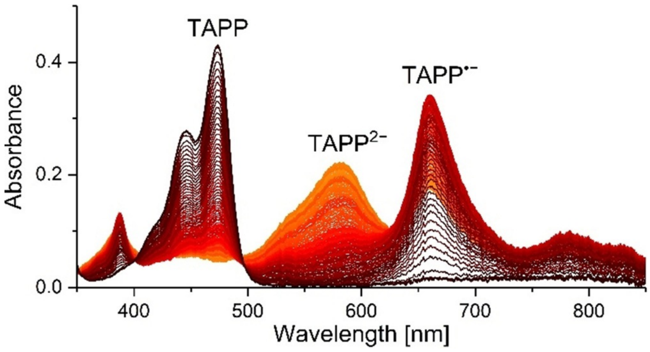

Figure 8. Absorption spectra of the two individual reduction steps of **5 a** in THF; voltage steps from 0 V (black) via −0.5 V (red) to −1.0 V (orange).

The two reduced TAPP species, TAPP$^{•−}$ and TAPP$^{2−}$, of **5 a**–**5 c** could also be isolated quantitatively by addition of one or two equivalents of KC_8, respectively (Scheme 5). The radical monoanionic TAPP-compounds were characterized by EPR (Figure 9), which for all derivatives possess a *g*-factor of 2.004, which is to be expected for radical organic compounds. Unfortunately, hyperfine couplings were only partially resolved precluding a complete simulation of the spectra.

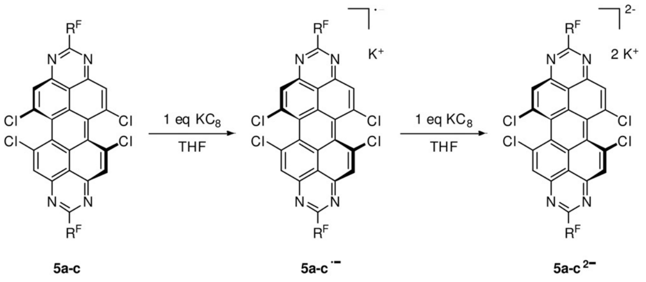

Scheme 5. Reduction of **5 a**–**c** to the radical monoanionic (**5 a**—**c**$^{•−}$) or diamagnetic dianionic TAPP (**5 a**–**c**$^{2−}$) using KC_8.

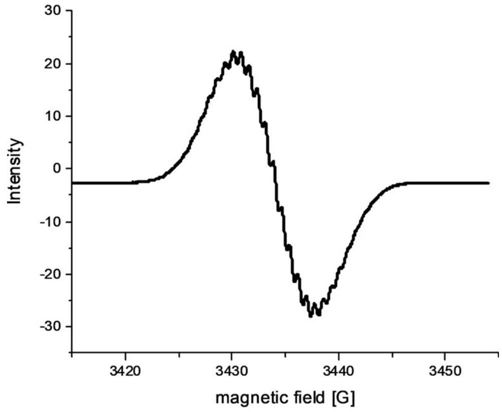

Figure 9. EPR-spectrum (THF, r.t.) of **5 b**.

None of the radical monoanions showed any signs of degradation under inert atmosphere, and even under ambient conditions the radicals only degraded very slowly, over a period of weeks, in the solid state. The insertion of the second electron led to a diamagnetic species, which allowed the compounds to be characterized by standard NMR methods, performed exemplarily for compound **5 a**. Both ^{1}H NMR spectra and ^{19}F NMR spectra display a shift of their signals to a higher field probably due to the enhanced electronic shielding by the additional electrons (Supporting Information). Also, the UV/Vis absorption spectra were recorded for each species, which reproduced the results of the spectroelectrochemical investigation depicted in Figure 8 (Supporting Information).

Bay-chlorinated TAPPs as n-channel semiconductors

Ortho-substituted TAPP derivatives have been successfully employed as semiconductors in n-channel organic TFTs, exhibiting electron mobilities of up to 0.17 cm^{2}V^{-1}s^{-1}.[63] In analogy, the *bay*-substituted TAPPs **5 a**–**c** were evaluated in bottom-gate, top-contact TFTs with a vacuum-deposited semiconductor layer (Table 5). The TFTs consisted of a doped silicon substrate that also served as a common gate electrode, a stack of thermally grown SiO_2, atomic-layer-deposited Al_2O_3 and a self-assembled monolayer (SAM) of *n*-tetradecylphosphonic acid as the gate dielectric, and shadow-mask-patterned Au top contacts (a detailed description of the fabrication process can be

Table 5. Summary of the transistor parameters electron field-effect mobility (μ_n), on/off current ratio (I_{on}/I_{off}), threshold voltage (V_{th}), subthreshold swing (*SS*) and temperature (*T*) measured under ambient conditions.

	I_{on}/I_{off}	V_{th}[V]	*SS* [V dec^{-1}]	*T* [°C]	μ_n [cm^2 V s^{-1}]
5 a	10^4	6	1.9	70	0.002
5 b	10^4	19	2.8	40	0.003
5 c	10^4	13	4.4	90	0.001

found in the Supporting Information). In all cases, n-channel semiconducting behavior was observed, with electron mobilities of 0.001 to 0.003 cm^2 V^{-1} s^{-1}.

The atomic force microscopy (AFM) images of the vacuum-deposited TAPP films reveal a low tendency of self-organization. The films of **5 a** and **5 c** are essentially amorphous, and only **5 b** shows a locally crystalline structure in certain areas of the image (Figure 10), which may explain the relatively low electron mobilities.

Figure 10. Atomic force microscopy (AFM) images of vacuum-deposited films of **5 a** (left), **5 b** (middle) and **5 c** (right).

In all cases, variation of the substrate temperature during the semiconductor deposition did not lead to an improvement of the self-organization of the material. On the other hand, the reduced tendency to pack in tight units, however, may open opportunities for the TAPP chemistry to explore new fields of applications. Also, the increased solubility associated with the reduced packing density is expected to be beneficial for solution processing.

Ortho- versus *bay*-substitution

To further understand the different influence of *ortho*- and *bay*-substitution in TAPP derivatives, the two core-chlorinated TAPP isomers **5 c** and **II** shall be compared. The absorption maxima at 474 nm (**5 c**) and 469 nm (**II**) of both isomers indicate that the bathochromic shift, induced by the chlorine substitution, is almost equally pronounced (Figure 11). However, the emission maximum of the *bay*-substituted derivative is red-shifted by 15 nm compared to the *ortho*-substituted TAPP, resulting in a Stokes shift for **5 c** of 936 cm^{-1} which is almost twice as large as observed for **II** (445 cm^{-1}). Additionally, the high fluorescence quantum yield of the *ortho*-chlorinated **II** (0.78) is reduced to 0.10 for the twisted *bay*-chlorinated TAPP **5 c** which appears to be characterized by more accessible internal degrees of freedom and thus enhanced non-radiative relaxation processes.

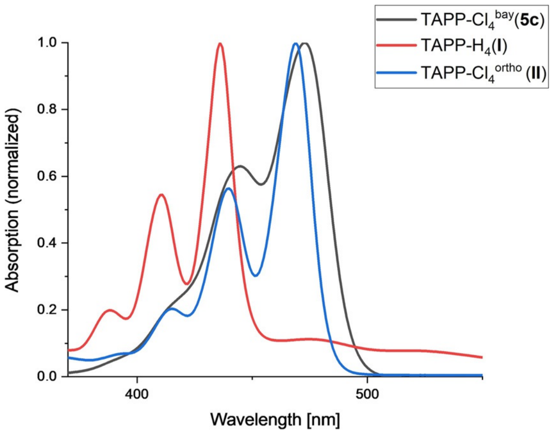

Figure 11. Absorption spectra of unsubstituted TAPP **I** (red), *ortho*-chlorinated TAPP **II** (blue) and *bay*-chlorinated TAPP **5 c** (black) in THF.

The comparison of the electrochemical properties also reveals some significant differences between **5 c** and **II** (Figure 12). The LUMO-level of both chlorinated isomers at −4.20 eV (**5 c**) and −4.03 eV (**II**) is significantly stabilized compared to the unsubstituted compound **I** (−3.66 eV), however, this effect is even more pronounced for the *bay*-substituted TAPP **5 c**. In contrast to the *ortho*-chlorinated derivative **II**, the *bay*-substitution additionally leads to a stabilization of the HOMO level, leading again to similar HOMO–LUMO gaps of 2.70 eV (**5 c**) and 2.63 eV (**II**). The electron affinity, which is also a key parameter in the evaluation of potential n-channel semiconductors, is higher for the *bay* substitution (3.31 eV) compared to the *ortho* substitution (3.09 eV). Overall, *bay*-chlorination leads to a greater stability of the anionic (radical) species compared to the *ortho*-substituted constitutional isomers.

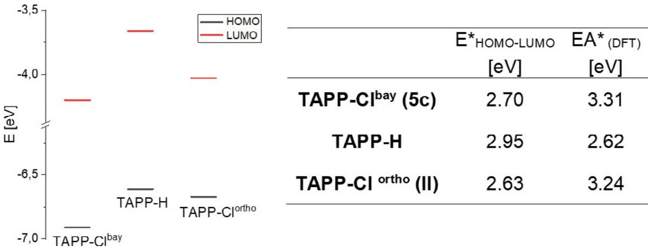

	E*$_{HOMO-LUMO}$ [eV]	EA* $_{(DFT)}$ [eV]
TAPP-Cl^{bay} (5c)	2.70	3.31
TAPP-H	2.95	2.62
TAPP-Cl ^{ortho} (II)	2.63	3.24

Figure 12. Calculated HOMO- and LUMO-levels (left) and HOMO–LUMO-gaps and EA (right) of **I**, **II** and **5 c**.

Whereas both, the photophysical and the electronic properties are similar for both TAPP-Cl isomers, the change of molecular geometry resulting from the different substitution patterns, is significant. Whereas the planar peropyrene core is barely affected by the *ortho*-substitution, the steric repulsion of the *bay* substituents leads to a large twist of approximately 30 degrees between the two subunits of the TAPP. This difference in molecular structure gives rise to an organized and dense packing pattern in case of the *ortho*-substituted derivative **II** in its solid-state structure (with intermolecular distances of 3.38 Å), whereas this type of packing is disrupted for the *bay*-substituted derivative **5 c** leading to reduced electron mobilities while the molecular redox properties are virtually unchanged. Conversely, the reduced long-range order, leads to a significantly increased solubility and potential processability of the *bay*-substituted molecules.

Conclusions

In this study we have expanded the chemistry of tetraazaperopyrenes (TAPPs) to include non-planar *bay*-chlorinated derivatives. This required a new synthetic strategy which was based on previous work in perylene chemistry and required the introduction of the condensed pyrimidine units to the central perylene core in the final reaction steps. As expected from previous studies of perylene bisimides, the *bay*-chlorinated TAPPs possess a twisted aromatic core due the steric pressure of the *bay*-substituents. In contrast to the previously studies *ortho*-substituted TAPPs, these new compounds allowed facile reduction to the monoanionic radical, which was found to be remarkably stable at ambient conditions. Further reduction gave thermally stable dianionic species which were characterized in solution. Both anionic species were characterized by UV/Vis, EPR and NMR spectroscopy, and theoretical modelling. The present work allows for the first time not only to fine-tune the electronic properties of TAPPs, but simultaneously adjust the geometric properties in a complementary fashion.

Experimental Section

The syntheses were performed under dried argon in standard Schlenk glassware, which was flame-dried prior to use. Solvents were dried according to standard procedures. The ^{1}H-,^{13}C- and ^{19}F-NMR spectra were recorded with Bruker AVANCE 400 and 600II+ spectrometers equipped with variable-temperature units. ^{1}H signals ($CDCl_3$: 7.26 ppm, [D_8]THF: 1.72 ppm/3.58 ppm, [D_6]DMSO: 2.50 ppm) and ^{13}C-signals ($CDCl_3$: 77.16 ppm, [D_8]THF: 67.21 ppm/25.31 ppm, [D_6]DMSO: 39.52 ppm) were referenced according to standard literature values.[64] The MALDI mass spectra were obtained from a Bruker apex-Qe FT-ICR spectrometer and a Bruker Autoflex Speed MALDI-TOF spectrometer. The absorption spectra were recorded on a Cary 500 UV/Vis/NIR spectrophotometer and were baseline and solvent corrected. Emission spectra were measured on a Varian Cary Eclipse Spectrophotometer. Description how Fluorescence quantum yields were obtained is explained in detail in the Supporting Information. Cyclic voltammetry was conducted using a standard commercial electrochemical analyser in a three-electrode single-component cell under inert atmosphere. The working electrode consists of a platinum disk, the counter electrode of a platinum wire and a saturated calomel electrode was used as a reference electrode. As internal reference ferrocene was used in all cases. As supporting electrolyte 0.1 M tetrabutylammonium hexafluorophosphate was used.

3,4,9,10-Tetrabromo-1,6,7,12-tetrachloroperylene (**1**) was synthesized according to the literature procedures.[1] All other starting materials were obtained commercially and used without further purification.

Preparation of compound 2

3,4,9,10-Tetrabromo-1,6,7,12-tetrachloroperylene (2.00 g, 2.83 mmol, 1 equiv.) was suspended in THF (200 mL) and *n*-butyllithium (7.94 mL, 2.5 M in hexane, 19.8 mmol, 7 equiv.) were added dropwise at −78 °C. After stirring at this temperature for one hour a solution of Tosyl azide (5.59 g, 28.4 mmol, 10 equiv.) in THF (5 mL) was added dropwise and the reaction mixture was allowed to warm up to r.t. overnight. After the addition of H_2O (30 mL), the phases were separated and the aqueous phase was extracted with DCM (3×100 mL). The united organic phases were dried over Na_2SO_4 and evaporation of the solvent gave the crude product, which was further washed with MeOH, acetonitrile and pentane to yield **2** as a red solid (0.75 g, 1.35 mmol, 66 %). ^{1}H NMR (600.13 MHz, $CDCl_3$ 295 K): δ [ppm] = 7.35 (s, 4 H). ^{13}C NMR (150.90 MHz, $CDCl_3$ 295 K): δ [ppm] = 114.6, 119.4, 122.1, 133.6, 136.6, 136.7.

Preparation of compound 3

Sodium borohydride (0.221 g, 5.85 mmol, 2.7 equiv.) was added to a solution of **2** (1.20 g, 2.17 mmol, 1 equiv.) in THF (72 mL) and MeOH (6 mL). The reaction mixture was stirred at r.t. for two hours. The reaction was quenched by the addition of 2 M HCl (1.20 mL), stirred for 30 minutes and subsequently aqueous 2 M NaOH (1.20 mL) was added. The solvent was removed in vacuo and the remaining solid was washed with water, MeOH, acetonitrile and pentane and dried in vacuo to give **3** as a red solid (0.75 g, 1.67 mmol, 77 %). ^{1}H NMR (600.13 MHz, [D_8]THF, 295 K): δ [ppm] = 5.43 (s, 8 H), 6.65 (s, 4 H). ^{13}C-NMR (150.90 MHz, [D_6]DMSO 295 K): δ [ppm] = 113.4, 123.5, 125.8, 136.4, 146.5, 159.5. HRMS (MALDI$^-$): calcd for $C_{20}H_{12}{}^{35}Cl_3{}^{37}Cl_1N_4$ $[M]^{+\cdot}$:.449.9787, found: 449.9781.

Preparation of compound 4

MnO_2 (3.00 g, 34.5 mmol, 20.7 equiv.) was added to a solution of **3** (0.75 g, 1.67 mmol, 1 equiv) in THF (250 mL). After stirring for one hour at r.t., the reaction mixture was filtered over Celite and the solvent was removed in vacuo to give the product **3** as a green solid (0.72 mg, 1.67 mmol, 96 %).^{1}H NMR (600.13 MHz, [D_6]DMSO, 295 K): δ [ppm] = 7.30 (s, 4 H), 9.19 (bs, 4 H), 10.48 (bs, 2 H). ^{13}C NMR (150.90 MHz, [D_6]DMSO, 295 K): δ [ppm] = 101.2, 122.8, 125.0, 134.6, 158.2. HRMS (MALDI$^-$): calcd for $C_{20}H_{10}{}^{35}Cl_3{}^{37}Cl_1N_4$ $[M]^{+\cdot}$: 447.9630; found: 447.9656.

Preparation of compound 5 a

Triethylamine (435 µL, 3.12 mmol, 2.8 equiv.) and trifluoroacetic anhydride (374 µL, 2.79 mmol, 2.5 equiv.) were added to a solution of DPDI-Cl (**4**) (500 mg, 1.12 mmol, 1 equiv.) in THF (10 mL) and the reaction mixture was refluxed for 72 h. After cooling to r.t., the volatiles were removed in vacuo and the crude mixture was separated by column chromatography (petroleum ether/ethyl acetate 10:1) to give the product **5 a** as a yellow solid (75 mg, 124 µmol, 11 %). ^{1}H NMR (600.13 MHz, $CDCl_3$ 295 K): δ [ppm] = 8.74 (s, 4 H). ^{13}C NMR (150.90 MHz, $CDCl_3$ 295 K): δ [ppm] = 112.7, 125.3, 126.1, 130.7, 141.1, 153.8. Residual ^{13}C signals of N-**C**-N- and **C**F_3-groups could not be detected due to coupling to fluorine groups and low solubility. ^{19}F NMR (376.27 MHz, $CDCl_3$ 295 K): δ [ppm] = −69.0 (s, 6 F). HRMS (MALDI$^-$): calcd for $C_{24}H_4{}^{35}Cl_3{}^{37}Cl_1F_6N_4$ $[M]^{-\cdot}$: 603.9065; found: 603.9059. Redox potentials measured against SCE in THF: $E_{red1} = -0.18$ V, $E_{red2} = -0.49$ V.

Preparation of compound 5 b:

Triethylamine (414 µL, 2.97 mmol, 2.8 equiv.) and pentafluoropropionic anhydride (526 µL, 2.66 mmol, 2.5 equiv) were added to a solution of DPDI-Cl (**4**) (476 mg, 1.06 mmol, 1 equiv.) in dioxane (10 mL) and the solution was refluxed for 72 h. After cooling to r.t., the solvent was removed in vacuo and the residue was washed thoroughly with water (200 mL). The crude compound was recrystallized in hot ethanol to afford **5 b** as a yellow solid (170 mg, 241 µmol, 23 %).^{1}H-NMR (600.13 MHz, $CDCl_3$ 295 K): δ [ppm] = 8.76 (s, 4 H). ^{13}C NMR (150.90 MHz, $CDCl_3$ 295 K): δ [ppm] = 112.6, 125.3, 126.1, 130.8, 141.1, 153.8, 156.1. Residual ^{13}C-signals of the perfluorinated pentyl groups could not be detected due to coupling to fluorine groups. ^{19}F NMR (376.27 MHz, $CDCl_3$ 295 K): δ [ppm] = −81.4 (t, $^{3}J_{F-F} = 1.75$ Hz, 6 F), −116.0 (bs, 4 F). HRMS (MALDI$^-$): calcd for $C_{26}H_4{}^{35}Cl_3{}^{37}Cl_1F_{10}N_4$ $[M]^{-}$: 703.9001; found: 703.9006. Redox potentials measured against SCE in THF: $E_{red1} = -0.18$ V, $E_{red2} = -0.49$ V.

Preparation of compound 5 c:

Triethylamine (217 µmol, 1.56 mmol, 2.8 equiv.) and perfluorobutyryl chloride (207 µl, 1.39 mmol, 2.5 equiv) were added to a solution of DPDI-Cl (**4**) (250 mg, 0.56 mmol, 1 equiv.) in THF (10 mL) and the solution was refluxed for 72 h. After cooling to r.t., the solvent was removed in vacuo and the residue was washed thoroughly with water (200 mL) and the crude product purified by column chromatography (petroleum ether/ethyl acetate 10:1) to give **5 c** as a yellow solid (54 mg, 76 µmol, 14 %). ^{1}H-NMR (600.13 MHz, $CDCl_3$ 295 K): δ [ppm] = 8.77 (s, 4 H). ^{13}C-NMR (150.90 MHz, $CDCl_3$ 295 K): δ [ppm] = 112.5, 125.3, 126.1, 130.8, 141.1, 153.7. Residual ^{13}C-signals of the N-**C**-N- and perfluorinated propyl-groups could not be detected due to coupling to fluorine groups. ^{19}F NMR (376.27 MHz, $CDCl_3$ 295 K): δ [ppm] = −80.1 (t, $^{3}J_{F-F} = 9.03$ Hz, 6 F), −114.0–114.1 (m, 4 F), −125.4 (bs, 4 F). HRMS (MALDI$^-$): calcd for $C_{28}H_4{}^{35}Cl_3{}^{37}Cl_1F_{14}N_4$ $[M]^{-}$: 803.8937; found: 803.8932. Redox potentials measured against SCE in THF: $E_{red1} = -0.19$ V, $E_{red2} = -0.49$ V.

Preparation of compound 5 d:

DPDI-Cl (**4**) (100 mg, 0.223 mmol, 1 equiv) was dissolved in 5 mL triethylorthoformiate and 1 mL of formic acid was added. The solution was stirred for 3 d at 110 °C. After cooling to r.t., the volatiles were removed in vacuo and residue was washed with water, MeOH and pentane. The pure compound **5 d** was isolated as a yellow powder (25 mg, 0.053 mmol, 24 %). ^{1}H NMR (600.13 MHz, $CDCl_3$ 295 K): δ [ppm] = 10.01 (s, 2 H), 8.59 (s, 4 H). ^{13}C NMR could not be measured due to low solubility. HRMS (MALDI$^-$): calcd for $C_{22}H_6{}^{35}Cl_3{}^{37}Cl_1N_4$ $[M]^{-}$: 467.9317; found: 467.9315. Redox potentials measured against SCE in THF: $E_{red1} = -0.383$ V, $E_{red2} = -0.681$ V.

Theoretical methods

Frontier orbitals and electron affinities: The DFT calculations to obtain orbital energies and electron affinities were carried out using ORCA 4.0.1 program package.[65] B3LYP was employed as functional;[66,67] a def2-SVP basis set was used for all atoms during geometry optimizations.[68,69] Every optimization was verified by frequency calculations. All other properties were calculated using a def2-QZVPP basis set.[70]

Vertical transitions: Calculations of the vertical excitation energies (VEE) and vertical de-excitation energies (VDE), employing B3LYP together with the def2-TZVPP basis, have been carried out using the Turbomole program package V7.2[71,72] using default convergence criteria for both the response equations and the geometry convergence. Accurate geometries for the Franck-Condon simulations were obtained with tightened thresholds of 10^{-9} and employing D_2 symmetry.[48] The calculations of the vibronic (Franck–Condon) spectra were conducted using the HOTFCHT program.[73–75]

Interconversion energies: The geometries and their relative energies have been computed using the Turbomole program V7.2. PBE0 was employed as functional together with def2-TZVP basis and the RI approximation (RI-J). The stationary points were verified with analytical second derivatives.

Acknowledgements

This work has been supported by the Deutsche Forschungsgemeinschaft (DFG) within the collaborative research centre SFB1249 "*N*-Heteropolycycles as Functional Materials" (Projects A02, B07, and C01).

Conflict of interest

The authors declare no conflict of interest.

Keywords: halogens · perylenes · radicals · synthetic methods · UV/Vis spectroscopy

[1] W. Herbst, K. Hunger, *Industrial Organic Pigments*, Wiley-VCH Verlag, Weinheim, **2004**.
[2] F. Würthner, *Chem. Commun.* **2004**, *0*, 1564 – 1579.
[3] F. Würthner, C. R. Saha-Möller, B. Fimmel, S. Ogi, P. Leowanawat, D. Schmidt, *Chem. Rev.* **2016**, *116*, 962 – 1052.
[4] C. Huang, S. Barlow, S. R. Marder, *J. Org. Chem.* **2011**, *76*, 2386 – 2407.
[5] X. Zhan, A. Facchetti, S. Barlow, T. J. Marks, M. A. Ratner, M. R. Wasielewski, S. R. Marder, *Adv. Mater.* **2011**, *23*, 268 – 284.
[6] R. Jiang, Z. Xue, Y. Lee, Z. Qin, Y. Li, D. Zhu, *Eur. J. Org. Chem.* **2014**, *23*, 5004 – 5009.
[7] C. Li, H. Wonneberger, *Adv. Mater.* **2012**, *24*, 613 – 636.
[8] D.-J. Liaw, K.-L. Wang, Y.-C. Huang, K.-R. Lee, J.-Y. Lai, C.-S. Ha, *Prog. Polym. Sci.* **2012**, *37*, 907 – 974.
[9] W. Jiang, Y. Li, Z. Wang, *Acc. Chem. Res.* **2014**, *47*, 3135 – 3147.
[10] Y. Avlasevich, C. Li, K. Müllen, *J. Mater. Chem.* **2010**, *20*, 3814 – 3826.
[11] L. Chen, C. Li, K. Müllen, *J. Mater. Chem. C* **2014**, *2*, 1938 – 1956.
[12] N. Soh, T. Ueda, *Talanta* **2011**, *85*, 1233 – 1237.
[13] A. Nowak-Król, F. Würthner, *Org. Chem. Front.* **2019**, *6*, 1272 – 1318.
[14] M. Sun, K. Müllen, M. Yin, *Chem. Soc. Rev.* **2016**, *45*, 1513 – 1528.
[15] G. Zhang, J. Zhao, P. C. Y. Chow, K. Jiang, J. Zhang, Z. Zhu, J. Zhang, F. Huang, H. Yan, *Chem. Rev.* **2018**, *118*, 3447 – 3507.
[16] A. Nowak-Król, K. Shoyama, M. Stolte, F. Würthner, *Chem. Commun.* **2018**, *54*, 13763.
[17] C. Yan, S. Barlow, Z. Wang, H. Yan, A. K.-Y. Jen, S. R. Marder, X. Zhan, *Nat. Rev. Mater.* **2018**, *3*, 18003.
[18] F. Würthner, *Pure Appl. Chem.* **2006**, *78*, 2341 – 2349.
[19] M. Queste, C. Cadiou, B. Pagoaga, L. Giraudet, N. Hoffmann, *New J. Chem.* **2010**, *34*, 2537.
[20] F. Würthner, P. Osswald, R. Schmidt, T. E. Kaiser, H. Mansikkamaki, M. Könemann, *Org. Lett.* **2006**, *8*, 3765 – 3768.
[21] R. Schmidt, J. H. Oh, Y.-S. Sun, M. Deppisch, A.-M. Krause, K. Radacki, H. Braunschweig, M. Könemann, P. Erk, Z. Bao, F. Würthner, *J. Am. Chem. Soc.* **2009**, *131*, 6215 – 6228.
[22] P. Leowanawat, A. Nowak-Król, F. Würthner, *Org. Chem. Front.* **2016**, *3*, 537 – 544.
[23] M. J. Lin, M. Schulze, K. Radacki, F. Würthner, *Chem. Commun.* **2013**, *49*, 9107 – 9109.
[24] T. Teraoka, S. Hiroto, H. Shinokubo, *Org. Lett.* **2011**, *13*, 2532 – 2535.

[25] X. Li, H. Wang, J. A. Schneider, Z. Wei, W.-Y. Lai, W. Huang, F. Wudl, Y. Zheng, *J. Mater. Chem. C* **2017**, *5*, 2781 – 2785.
[26] W. Yue, W. Jiang, M. Böckmann, N. L. Doltsinis, Z. Wang, *Chem. Eur. J.* **2014**, *20*, 5209 – 5213.
[27] S. Nakazono, S. Easwaramoorthi, D. Kim, H. Shinokubo, A. Osuka, *Org. Lett.* **2009**, *11*, 5426 – 5429.
[28] G. Battagliarin, Y. Zhao, C. Li, K. Müllen, *Org. Lett.* **2011**, *13*, 3399 – 3401.
[29] G. Battagliarin, C. Li, V. Enkelmann, *Org. Lett.* **2011**, *13*, 3012 – 3015.
[30] J. Wu, D. He, L. Zhang, Y. Liu, X. Mo, J. Lin, H. J. Zhang, *Org. Lett.* **2017**, *19*, 5438 – 5441.
[31] N. Zink-Lorre, E. Font-Sanchis, Á. Sastre-Santos, F. Fernández-Lázaro, *Org. Chem. Front.* **2017**, *4*, 2016 – 2021.
[32] S. Seifert, D. Schmidt, F. Würthner, *Chem. Sci.* **2015**, *6*, 1663 – 1667.
[33] Y. Kumar, S. Kumar, S. Kumar Keshri, J. Shukla, S. S. Singh, T. S. Thakur, M. Denti, A. Facchetti, P. Mukhopadhyay, *Org. Lett.* **2016**, *18*, 472 – 475.
[34] M. Sadrai, G. R. Bird, J. A. Potenza, H. J. Schugar, *Acta Crystallogr. Sect. C* **1990**, *46*, 637.
[35] M. Gsänger, J. H. Oh, M. Könemann, H. W. Höffken, A. Krause, Z. Bao, F. Würthner, *Angew. Chem. Int. Ed.* **2010**, *49*, 740–743; *Angew. Chem.* **2010**, *122*, 752.
[36] T. Riehm, G. De Paoli, A. E. Konradsson, L. De Cola, H. Wadepohl, L. H. Gade, *Chem. Eur. J.* **2007**, *13*, 7317 – 7329.
[37] M. Matena, T. Riehm, M. Stöhr, T. A. Jung, L. H. Gade, *Angew. Chem. Int. Ed.* **2008**, *47*, 2414 – 2417; *Angew. Chem.* **2008**, *120*, 2448 – 2451.
[38] S. Blankenburg, E. Rauls, W. G. Schmidt, *J. Phys. Chem. Lett.* **2010**, *1*, 3266 – 3270.
[39] M. Matena, M. Stöhr, T. Riehm, J. Björk, S. Martens, M. S. Dyer, M. Persson, J. Lobo-Checa, K. Müller, M. Enache, et al., *Chem. A Eur. J.* **2010**, *16*, 2079 – 2091.
[40] J. Björk, M. Matena, M. S. Dyer, M. Enache, J. Lobo-Checa, L. H. Gade, T. A. Jung, M. Stöhr, M. Persson, *Phys. Chem. Chem. Phys.* **2010**, *12*, 8815 – 8821.
[41] S. C. Martens, T. Riehm, S. Geib, H. Wadepohl, L. H. Gade, *J. Org. Chem.* **2011**, *76*, 609 – 617.
[42] S. C. Martens, U. Zschieschang, H. Wadepohl, H. Klauk, L. H. Gade, *Chem. Eur. J.* **2012**, *18*, 3498 – 3509.
[43] S. Geib, S. C. Martens, M. Märken, A. Rybina, H. Wadepohl, L. H. Gade, *Chem. Eur. J.* **2013**, *19*, 13811 – 13822.
[44] S. Geib, U. Zschieschang, M. Gsänger, M. Stolte, F. Würthner, H. Wadepohl, H. Klauk, L. H. Gade, *Adv. Funct. Mater.* **2013**, *23*, 3866 – 3874.
[45] L. Hahn, S. Öz, H. Wadepohl, L. H. Gade, *Chem. Commun.* **2014**, *50*, 4941 – 4943.
[46] Y. Shi, H. Wei, Y. Liu, *J. Mol. Struct.* **2015**, *1083*, 65 – 71.
[47] L. Hahn, A. Hermannsdorfer, B. Günther, T. Wesp, B. Bühler, U. Zschieschang, H. Wadepohl, H. Klauk, L. H. Gade, *J. Org. Chem.* **2017**, *82*, 12492 – 12502.
[48] S. Höfener, B. Günther, M. E. Harding, L. H. Gade, *J. Phys. Chem. A* **2019**, *123*, 3160 – 3169.
[49] Y. Zagranyarski, L. Chen, D. Jänsch, T. Gessner, C. Li, K. Müllen, *Org. Lett.* **2014**, *16*, 2814 – 2817.
[50] A. Insuasty, S. Maniam, S. J. Langford, *Chem. Eur. J.* **2019**, *25*, 7058 – 7073.
[51] Z. Xie, F. Würthner, *Org. Lett.* **2010**, *12*, 3204 – 3207.
[52] P. Osswald, D. Leusser, D. Stalke, F. Würthner, *Angew. Chem. Int. Ed.* **2005**, *44*, 250 – 253; *Angew. Chem.* **2005**, *117*, 254 – 257.
[53] M. M. Safont-Sempere, P. Osswald, M. Stolte, M. Grüne, M. Renz, M. Kaupp, K. Radacki, H. Braunschweig, F. Würthner, *J. Am. Chem. Soc.* **2011**, *133*, 9580 – 9591.
[54] A. Nowak-Król, M. I. S. Röhr, D. Schmidt, F. Würthner, *Angew. Chem. Int. Ed.* **2017**, *56*, 11774 – 11778; *Angew. Chem.* **2017**, *129*, 11936 – 11940.
[55] M. M. Safont-Sempere, P. Osswald, K. Radacki, F. Würthner, *Chem. Eur. J.* **2010**, *16*, 7380 – 7384.
[56] M. M. Safont-Sempere, V. Stepanenko, M. Lehmann, F. Würthner, *J. Mater. Chem.* **2011**, *21*, 7201 – 7209.
[57] Z. Xie, V. Stepanenko, K. Radacki, F. Würthner, *Chem. Eur. J.* **2012**, *18*, 7060 – 7070.
[58] E. Fron, G. Schweitzer, P. Osswald, F. Würthner, P. Marsal, D. Beljonne, K. Müllen, F. C. De Schryver, M. Van der Auweraer, *Photochem. Photobiol. Sci.* **2008**, *7*, 1509 – 1521.
[59] P. Osswald, F. Würthner, *J. Am. Chem. Soc.* **2007**, *129*, 14319 – 14326.
[60] I. Seguy, P. Jolinat, P. Destruel, R. Mamy, H. Allouchi, C. Courseille, M. Cotrait, H. Bock, *ChemPhysChem* **2001**, *2*, 448 – 452.
[61] M. J. van Setten, F. Weigend, F. Evers, *J. Chem. Theory Comput.* **2013**, *9*, 232 – 246.
[62] B. C. Lin, C. P. Cheng, Z. P. M. Lao, *J. Phys. Chem. A* **2003**, *107*, 5241 – 5251.
[63] L. Hahn, F. Maaß, T. Bleith, U. Zschieschang, H. Wadepohl, H. Klauk, P. Tegeder, L. H. Gade, *Chem. Eur. J.* **2015**, *21*, 17691 – 17700.
[64] G. R. Fulmer, A. J. M. Miller, N. H. Sherden, H. E. Gottlieb, A. Nudelman, B. M. Stoltz, J. E. Bercaw, K. I. Goldberg, *Organometallics* **2010**, *29*, 2176 – 2179.
[65] F. Neese, *Wiley Interdiscip. Rev.: Comput. Mol. Sci.* **2012**, *2*, 73 – 78.
[66] A. D. Becke, *J. Chem. Phys.* **1993**, *98*, 5648 – 5652.
[67] A. D. Becke, *J. Chem. Phys.* **1993**, *98*, 1372 – 1377.
[68] C. Lee, W. Yang, R. G. Parr, *Phys. Rev. B* **1988**, *37*, 785 – 789.
[69] F. Weigend, M. Häser, H. Patzelt, R. Ahlrichs, *Chem. Phys. Lett.* **1998**, *294*, 143 – 152.
[70] F. Weigend, R. Ahlrichs, *Phys. Chem. Chem. Phys.* **2005**, *7*, 3297.
[71] *TURBOMOLE V7.2 2017*, A Development Of University Of Karlsruhe And Forschungszentrum Karlsruhe GmbH.
[72] R. Ahlrichs, M. Bär, M. Häser, H. Horn, C. Kölmel, *Chem. Phys. Lett.* **1989**, *162*, 165 – 169.
[73] R. Berger, C. Fischer, M. Klessinger, *J. Phys. Chem. A* **1998**, *102*, 7157 – 7167.
[74] R. Berger, M. Klessinger, *J. Comput. Chem.* **1997**, *18*, 1312 – 1319.
[75] H.-C. Jankowiak, J. L. Stuber, R. Berger, *J. Chem. Phys.* **2007**, *127*, 234101.

Manuscript received: July 26, 2019
Revised manuscript received: August 30, 2019
Accepted manuscript online: September 17, 2019
Version of record online: October 22, 2019

CHEMISTRY
A European Journal

Supporting Information

Twisting the TAPPs: *Bay*-Substituted Non-planar Tetraazaperopyrenes and their Reduced Anions

Benjamin A. R. Günther,[a] Sebastian Höfener,[b] Ute Zschieschang,[c] Hubert Wadepohl,[a] Hagen Klauk,[c] and Lutz H. Gade*[a]

chem_201903413_sm_miscellaneous_information.pdf

Table of Contents

The ^{1}H, ^{13}C and ^{19}F NMR Spectra of Compounds

Compound 2

^{1}H-NMR (600.13 MHz, $CDCl_3$, 295 K):

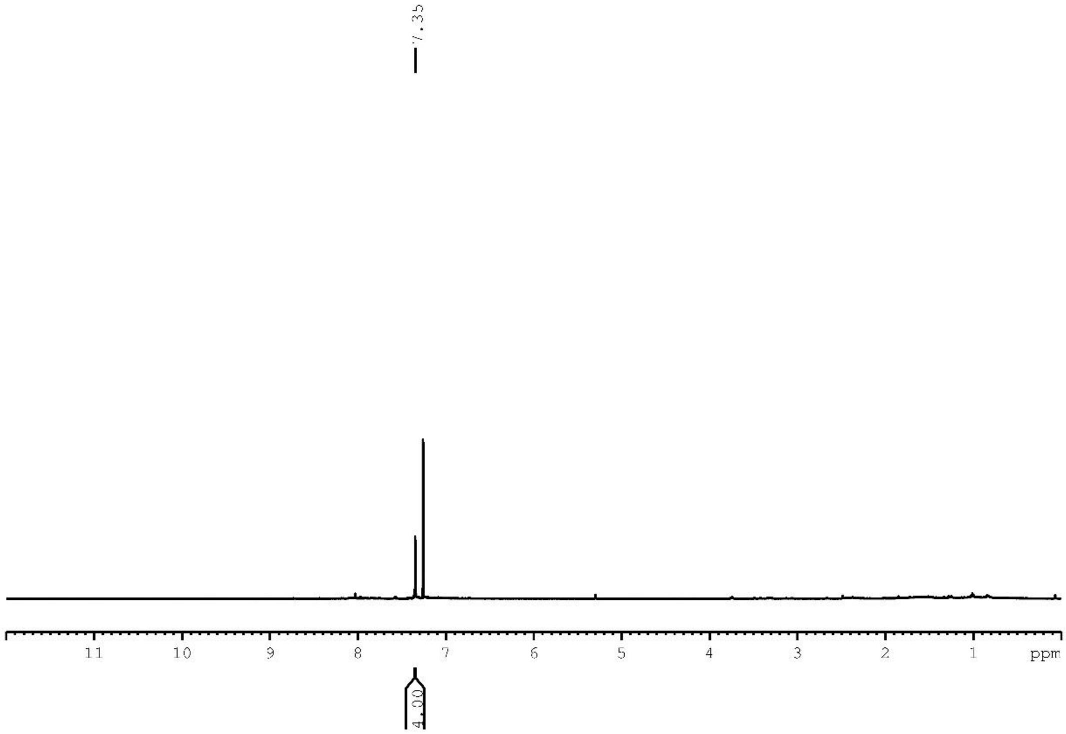

^{13}C-NMR (150.90 MHz, $CDCl_3$, 295 K):

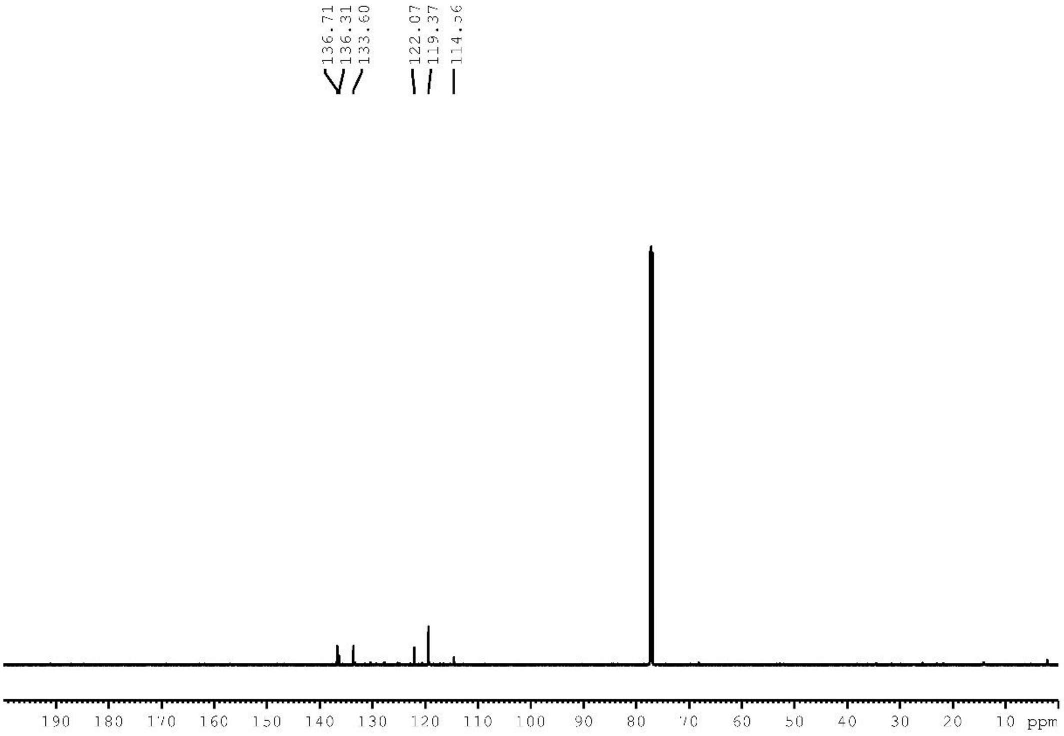

Compound 3

^{1}H-NMR (600.13 MHz, thf-d_8, 295 K):

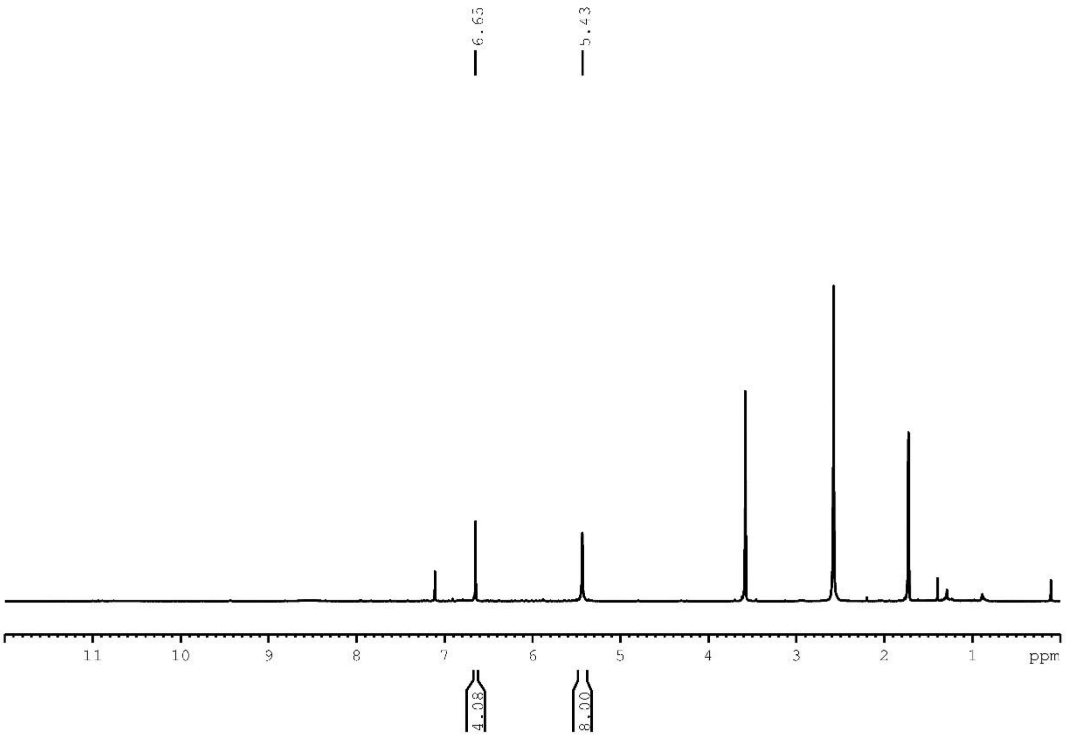

^{13}C-NMR (150.90 MHz, dmso-d$_6$, 295 K):

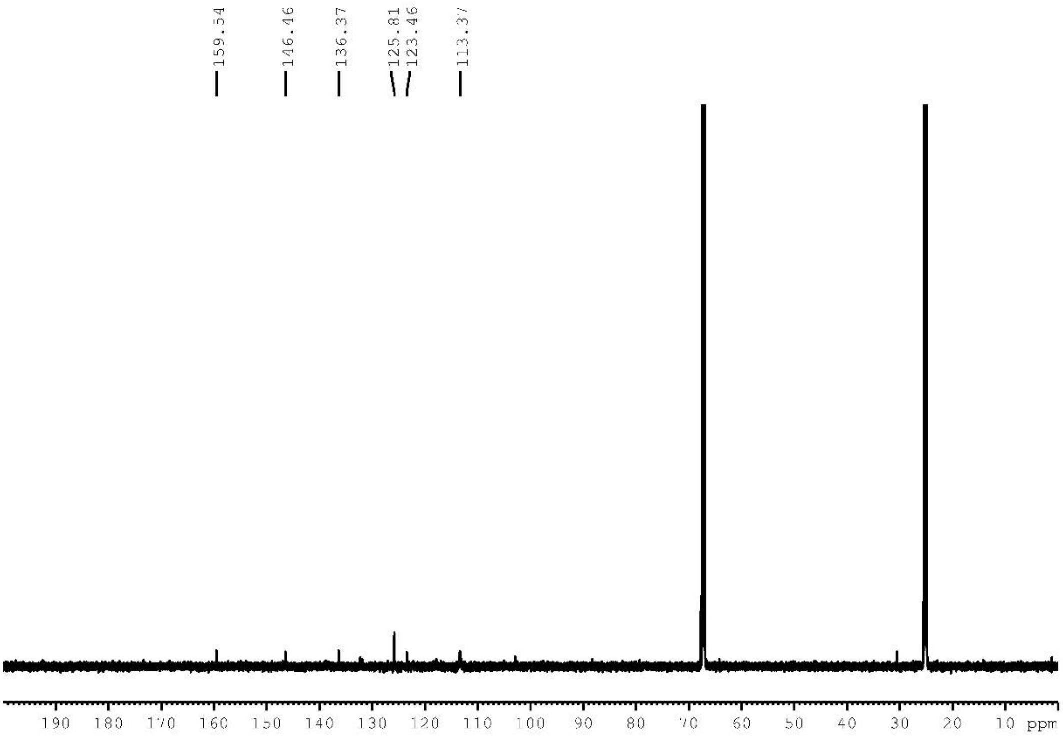

Compound 4

^{1}H-NMR (600.13 MHz, dmso-d$_6$, 295 K):

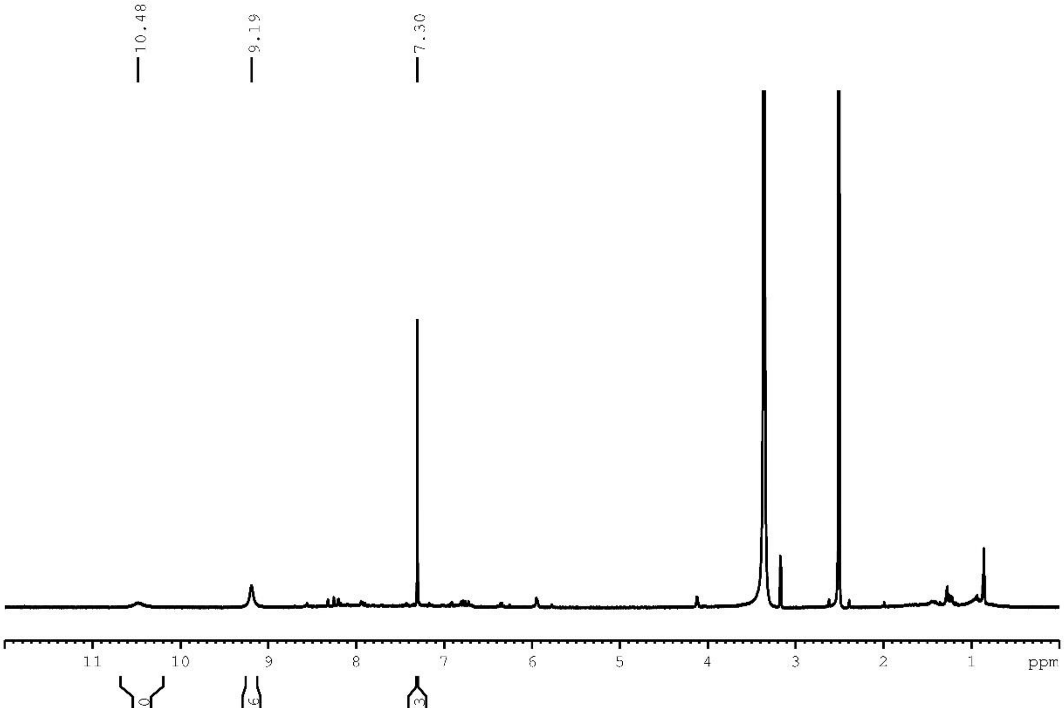

^{13}C-NMR (150.90 MHz, dmso-d_6, 295 K):

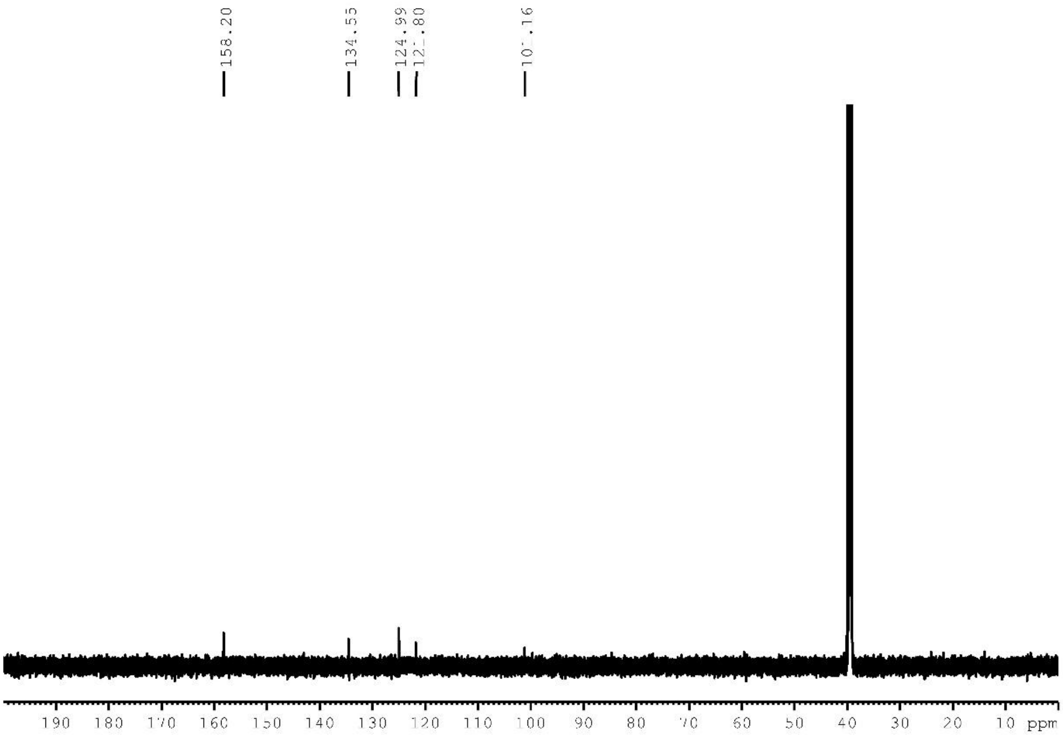

Compound 5a (CF_3-TAPP-Cl_4)

^{1}H-NMR (600.13 MHz, $CDCl_3$, 295 K):

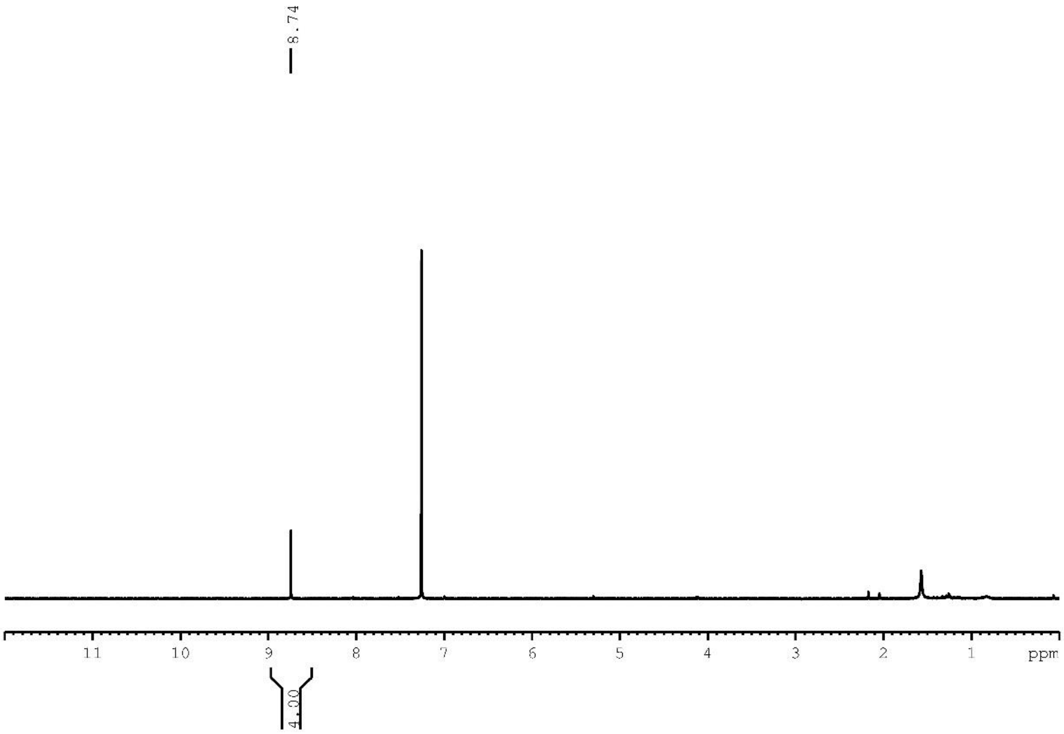

^{13}C-NMR (150.90 MHz, $CDCl_3$, 295 K):

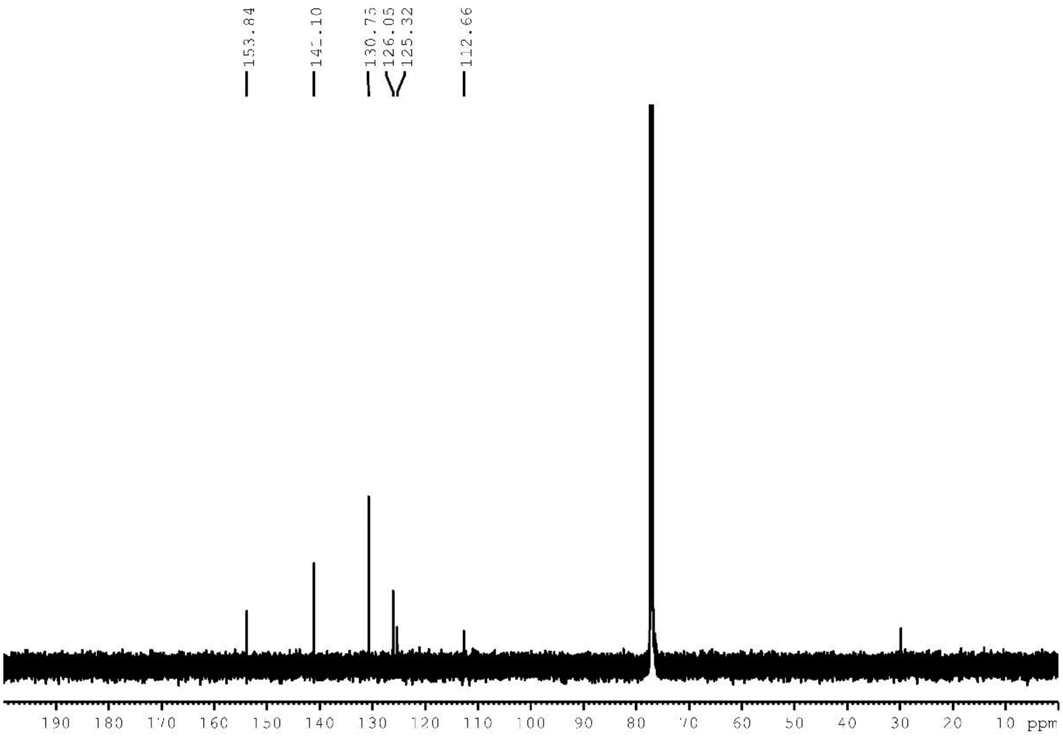

^{19}F-NMR (376.27 MHz, $CDCl_3$, 295 K):

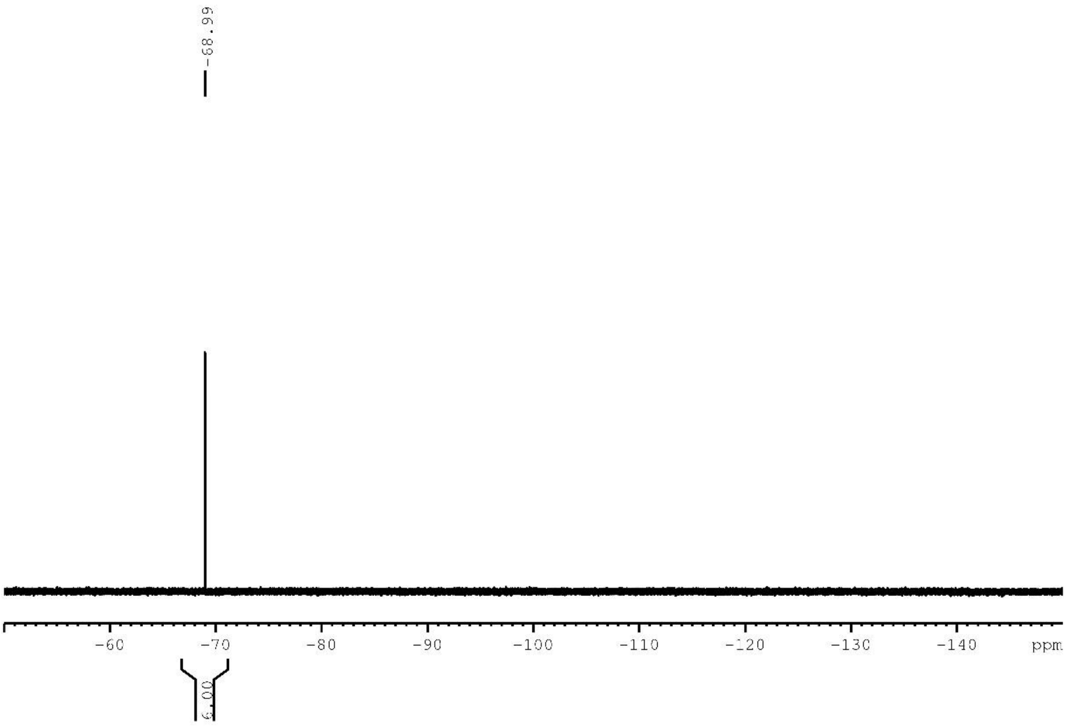

Compound 5b (C_2F_5-TAPP-Cl_4)

^{1}H-NMR (600.13 MHz, $CDCl_3$, 295 K):

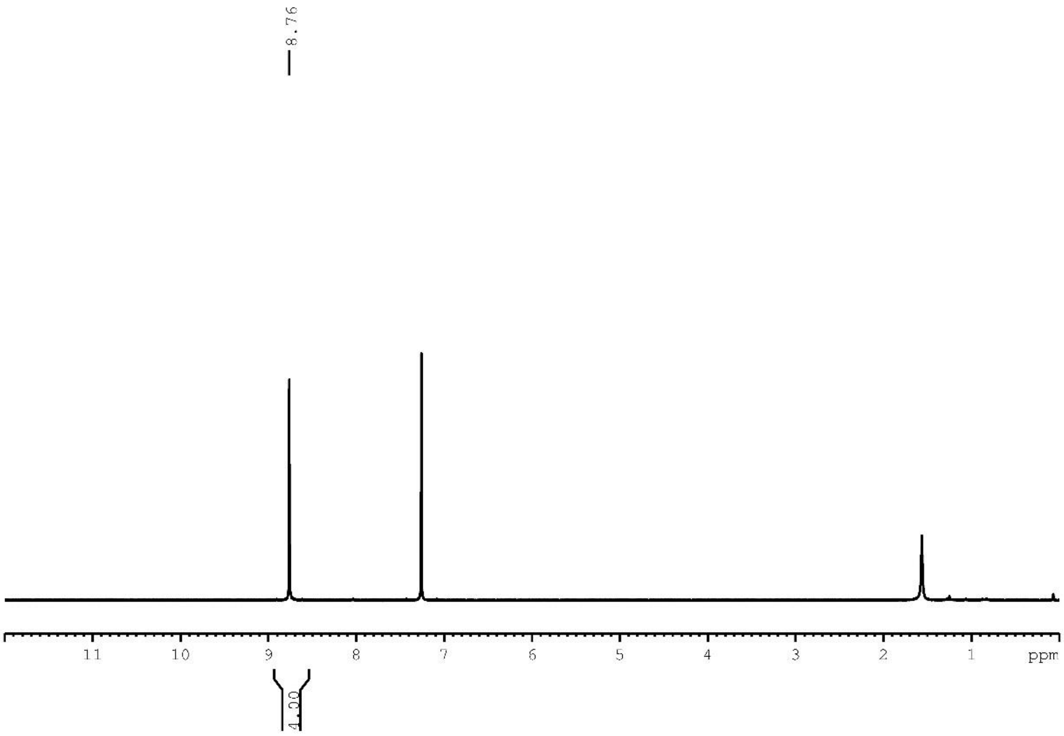

^{13}C-NMR (150.90 MHz, $CDCl_3$, 295 K):

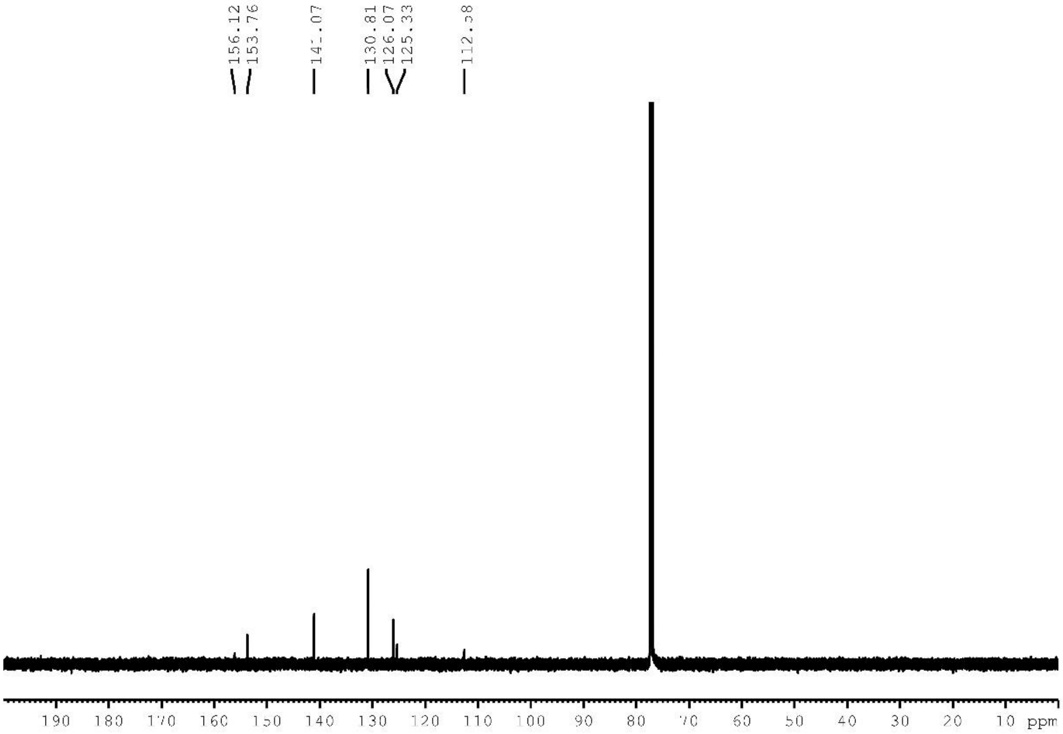

^{19}F-NMR (376.27 MHz, $CDCl_3$, 295 K):

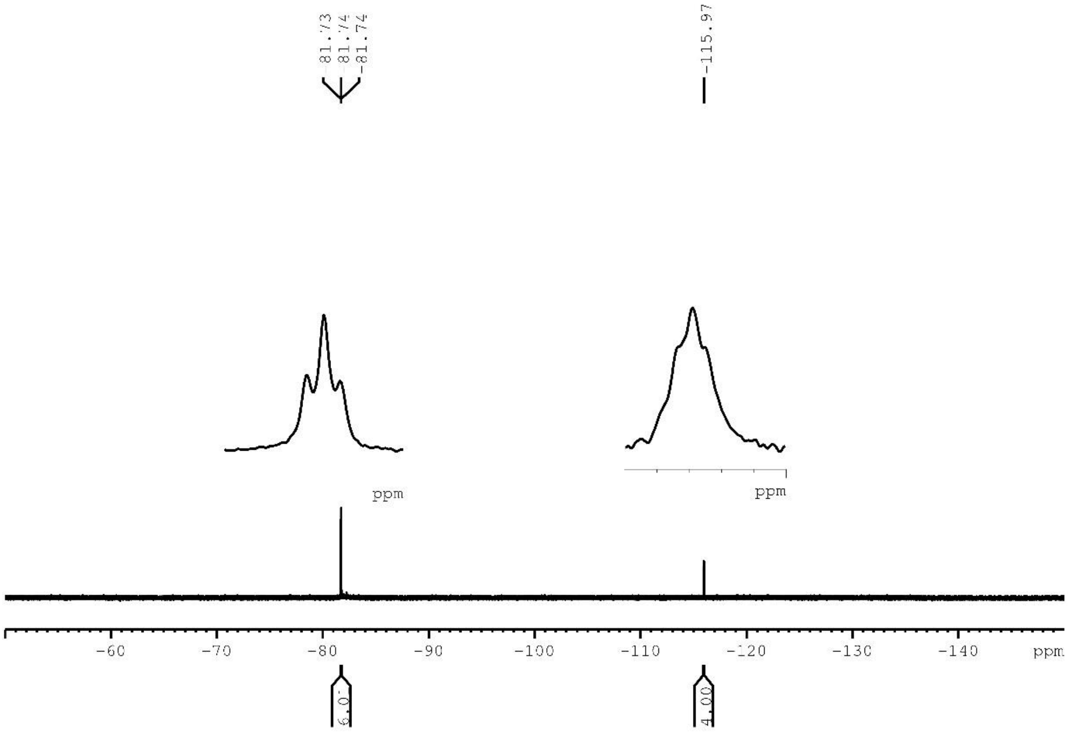

Compound 5c (C_3F_7-TAPP-Cl_4)

^{1}H-NMR (600.13 MHz, $CDCl_3$, 295 K):

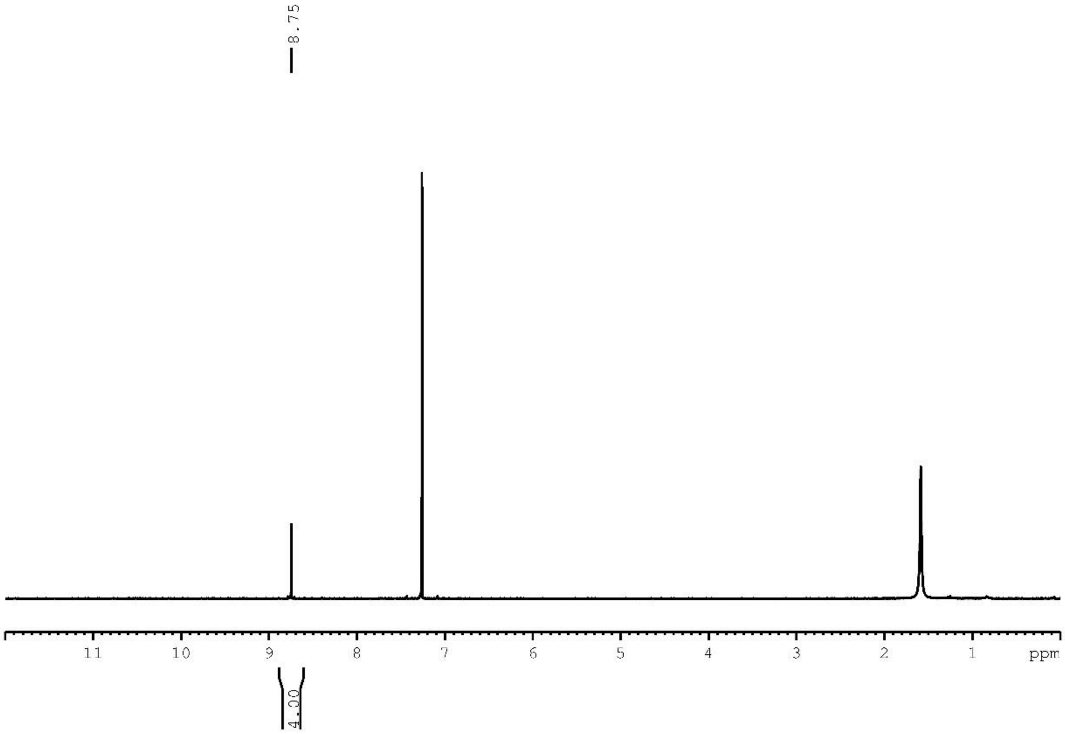

^{13}C-NMR (150.90 MHz, CDCl$_3$, 295 K):

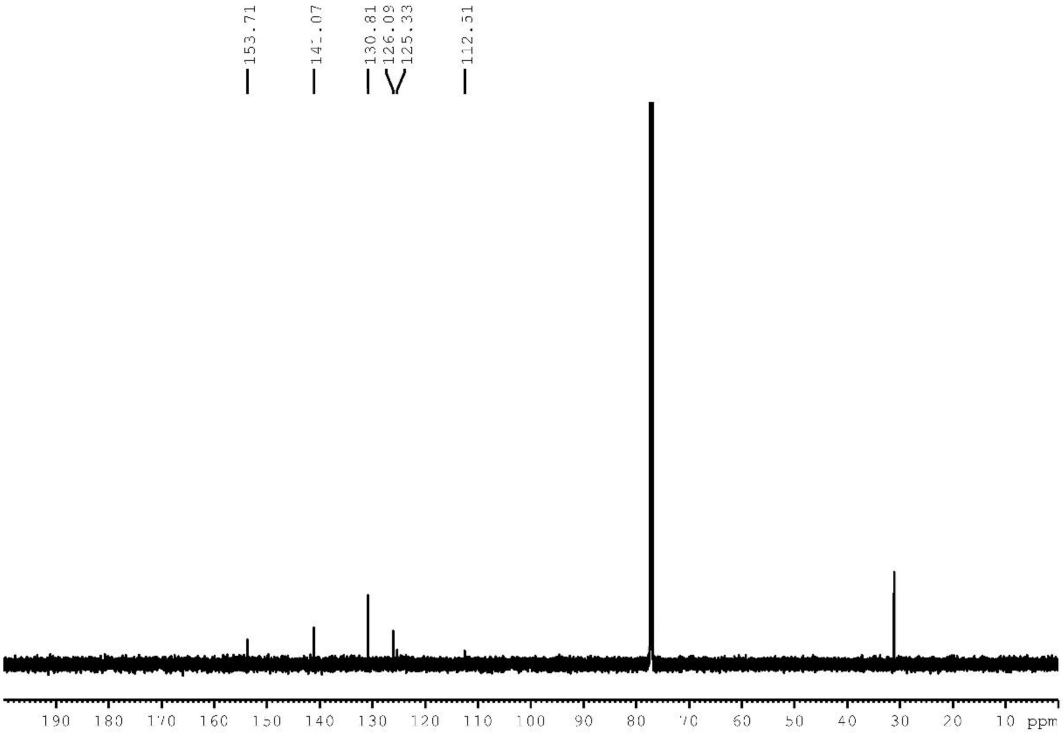

^{19}F-NMR (376.27 MHz, CDCl$_3$, 295 K):

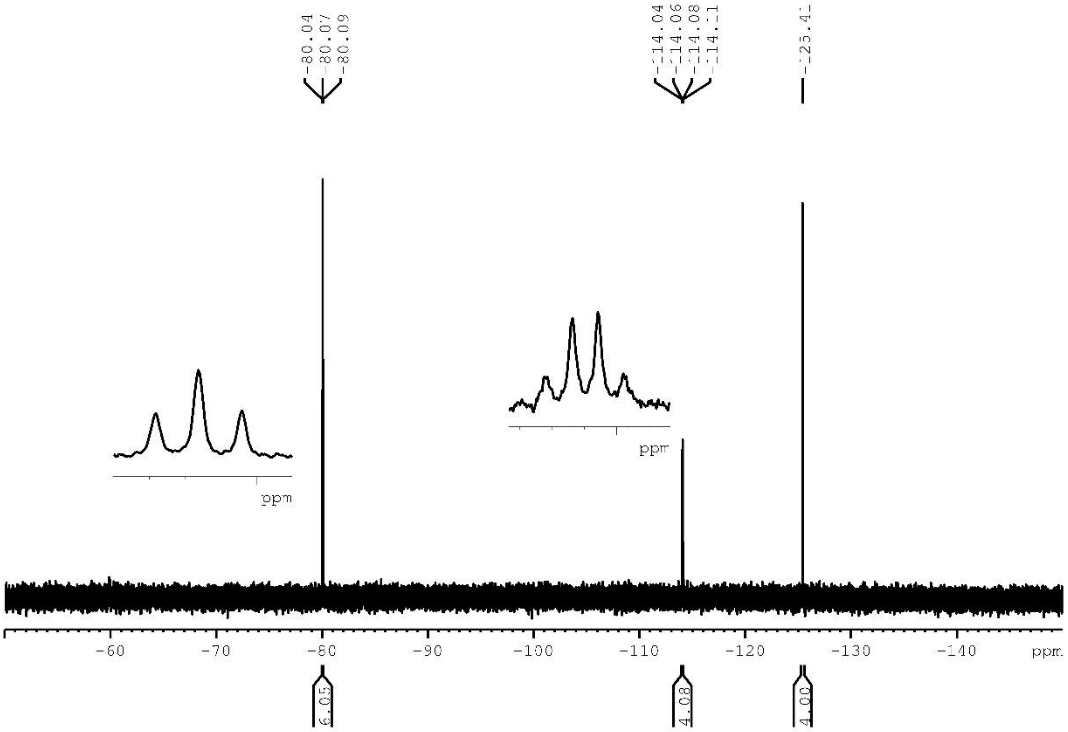

Compound 5d (H-TAPP-Cl_4)

^{1}H-NMR (600.13 MHz, $CDCl_3$, 295 K):

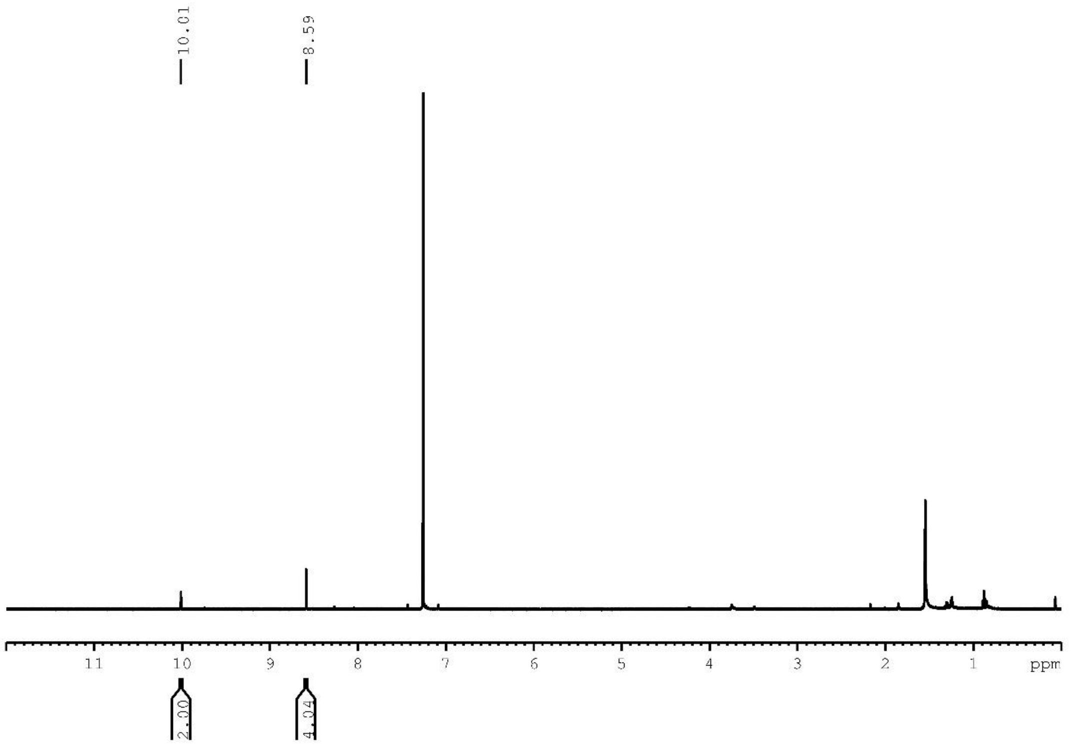

Absorption Spectra of Compounds 5a-d

Compound 5a (CF_3-TAPP-Cl_4)

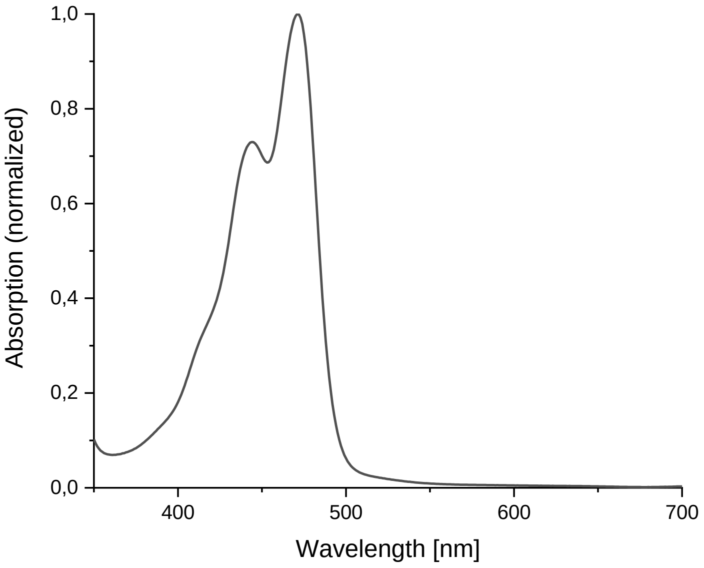

Compound 5b (C_2F_5-TAPP-Cl_4)

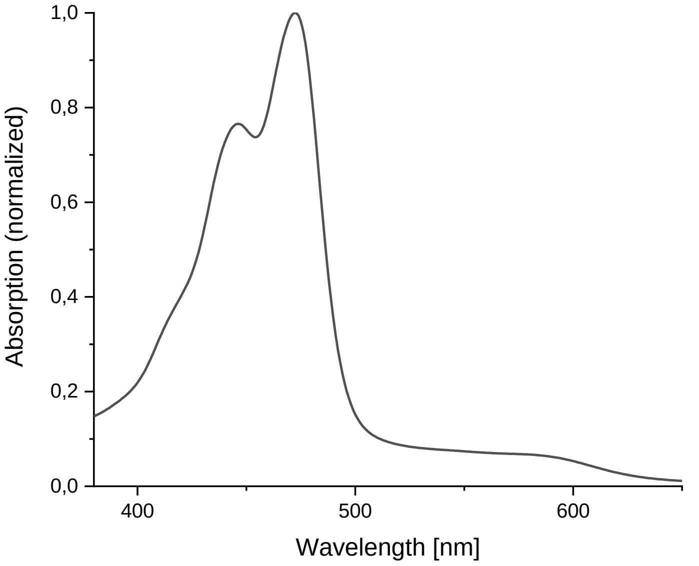

Compound 5c (C_3F_7-TAPP-Cl_4)

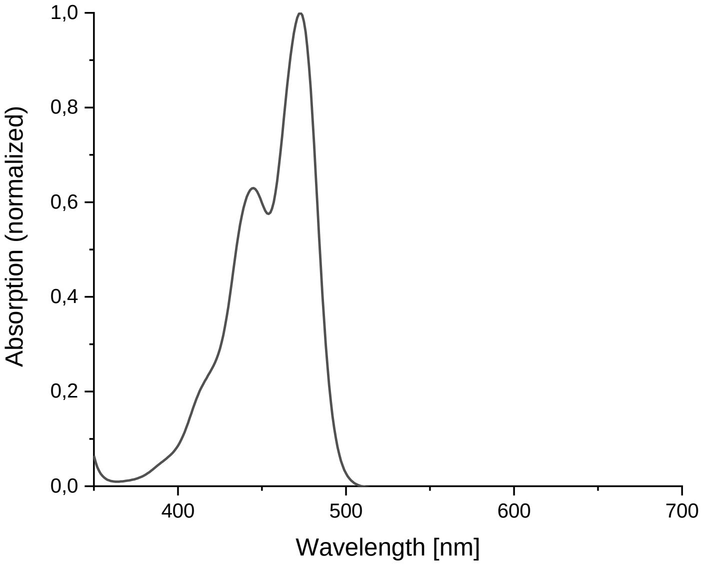

Compound 5d (H-TAPP-Cl_4)

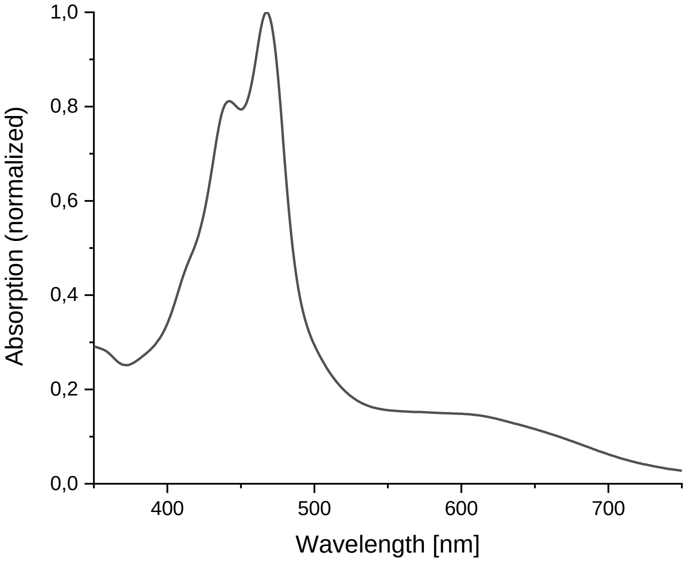

Emission Spectra of Compounds 5a-d

Fluorescence quantum yields were determined in dilute solutions (OD < 1 at the excitation wavelength) and referenced to Fluorescin by using equation (**1**). A is the absorbance at the excitation wavelength (λ), I is the intensity of the excitation light at (λ), n is the refractive index of the solvent, D is the integrated scripts and r and x refer to the reference and sample. All quantum yields were obtained at identical excitation wavelengths of sample and reference in order to cancel out the term $I(\lambda_r)/I(\lambda_x)$ of equation (**1**).

$$\textbf{(1)}\quad \boldsymbol{\Phi_x = \Phi_r \left(\frac{A_r(\lambda_r)}{A_x(\lambda_x)}\right)\left(\frac{I_r(\lambda_r)}{I_x(\lambda_x)}\right)\left(\frac{n_x^2}{n_r^2}\right)\left(\frac{D_x}{D_r}\right)}$$

Compound 5a (CF_3-TAPP-Cl_4)

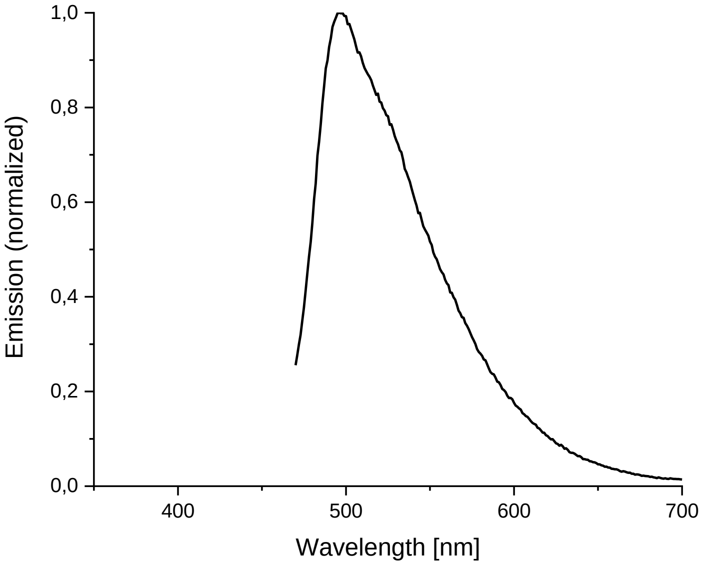

Compound 5b (C_2F_5-TAPP-Cl_4)

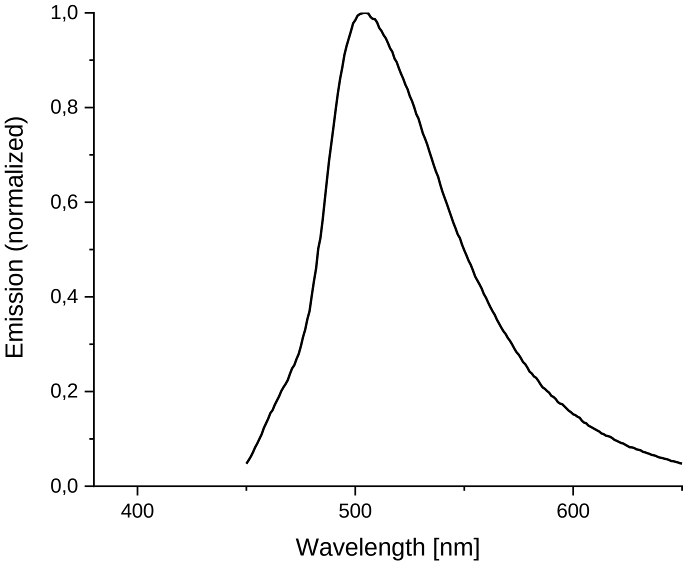

Compound 5c (C_3F_7-TAPP-Cl_4)

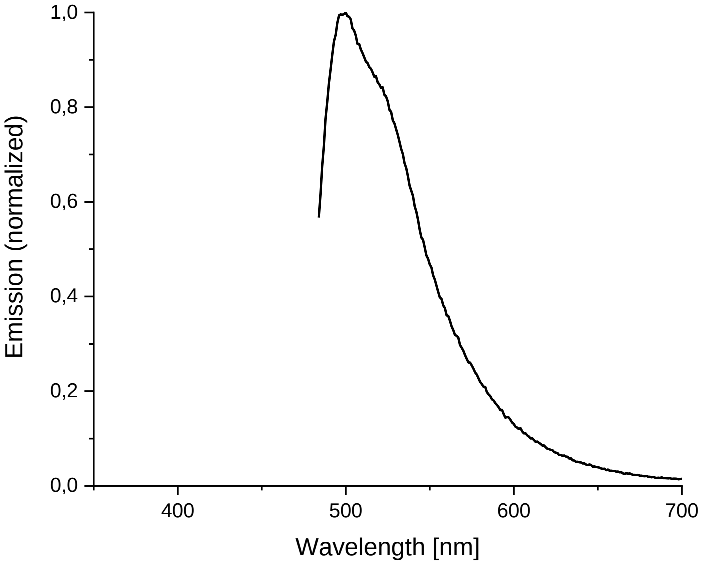

Compound 5d (H-TAPP-Cl_4)

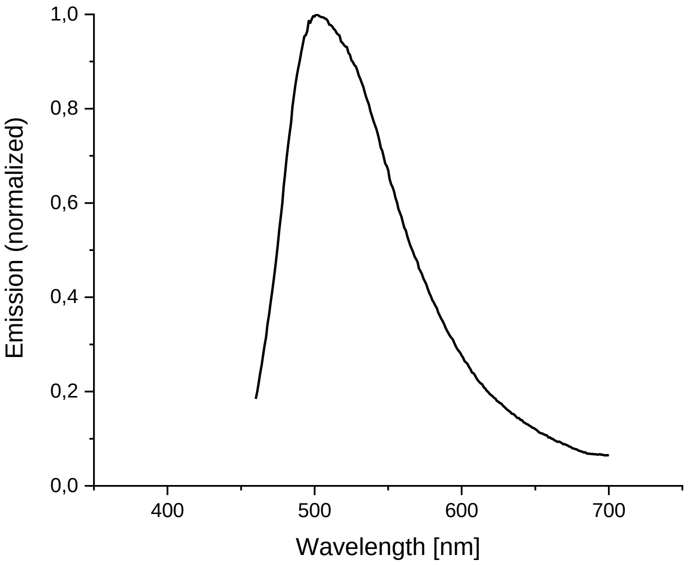

Cyclic Voltammograms of Compounds 5a-d

Compound 5a (CF_3-TAPP-Cl_4)

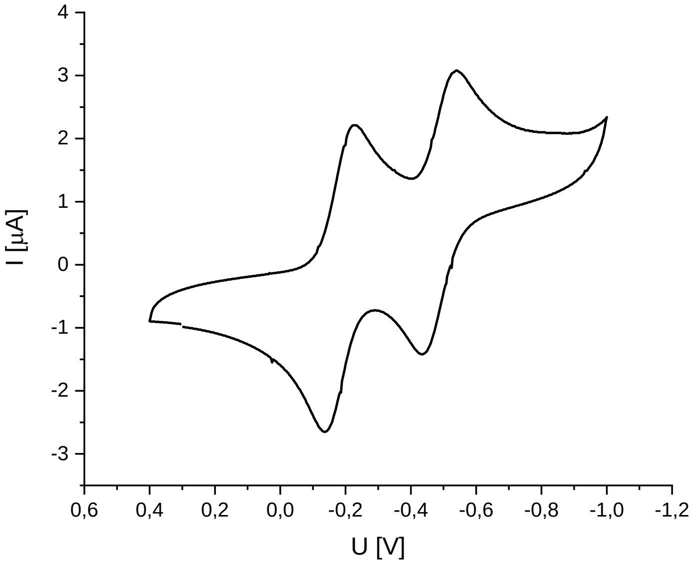

Compound 5b (C_2F_5-TAPP-Cl_4)

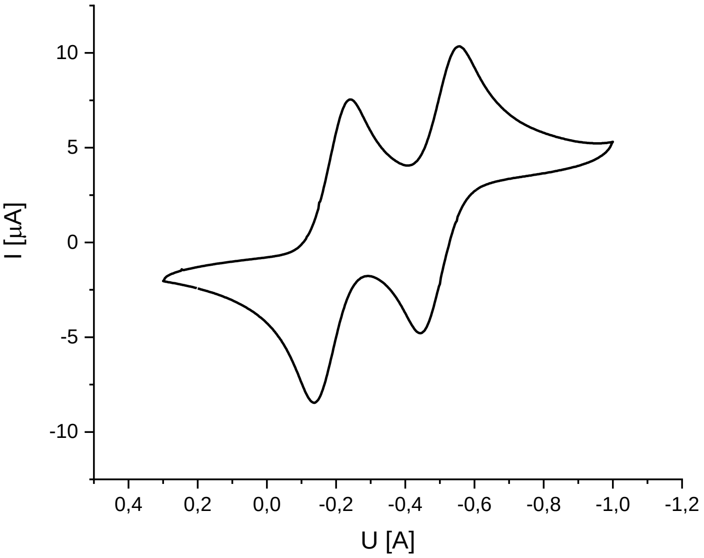

Compound 5c (C_3F_7-TAPP-Cl_4)

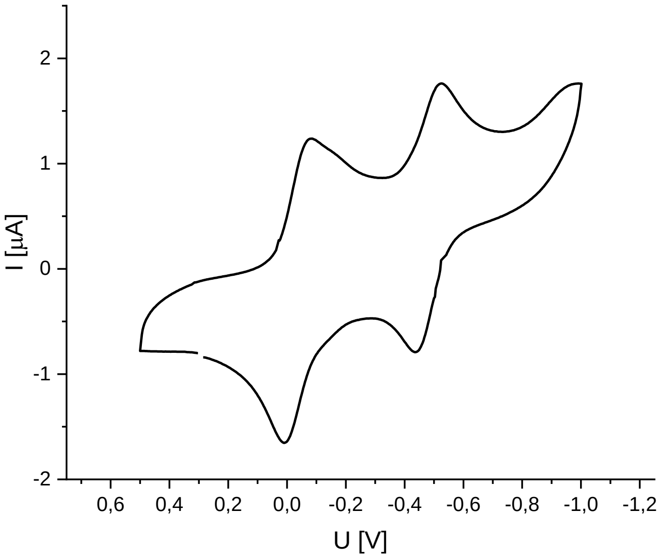

Compound 5d (H-TAPP-Cl_4)

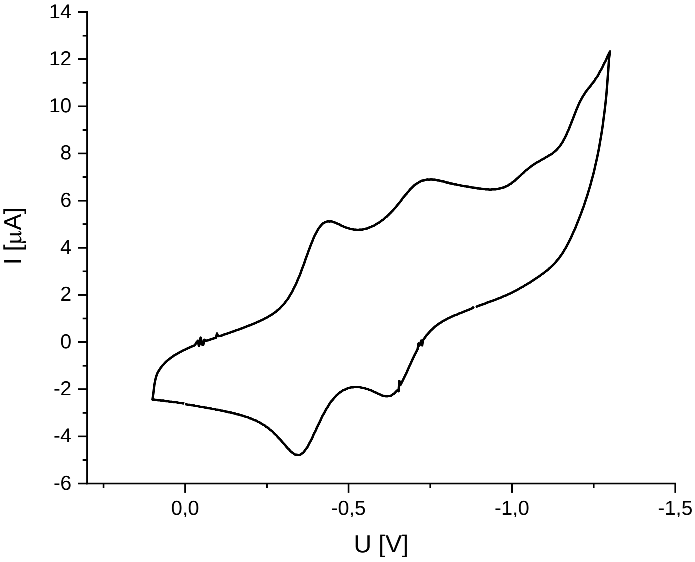

Characterization of Reduced Species

ESR-Spectra of Compounds 5a-c

Compound 5a (CF_3-TAPP-Cl_4)

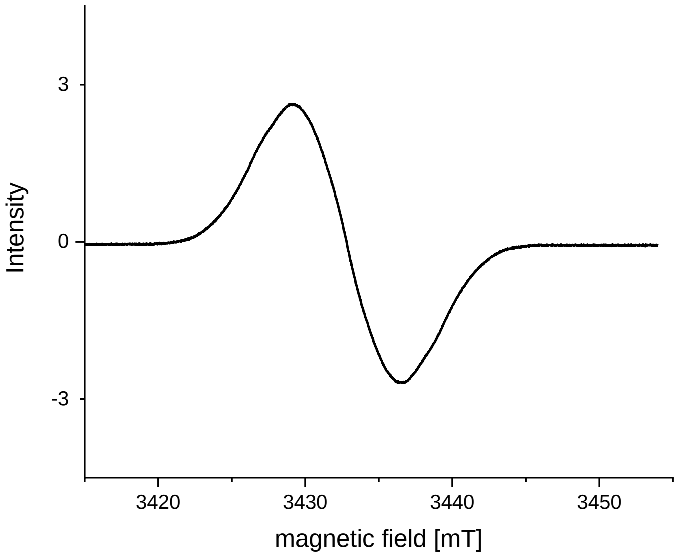

Compound 5b (C_2F_5-TAPP-Cl_4)

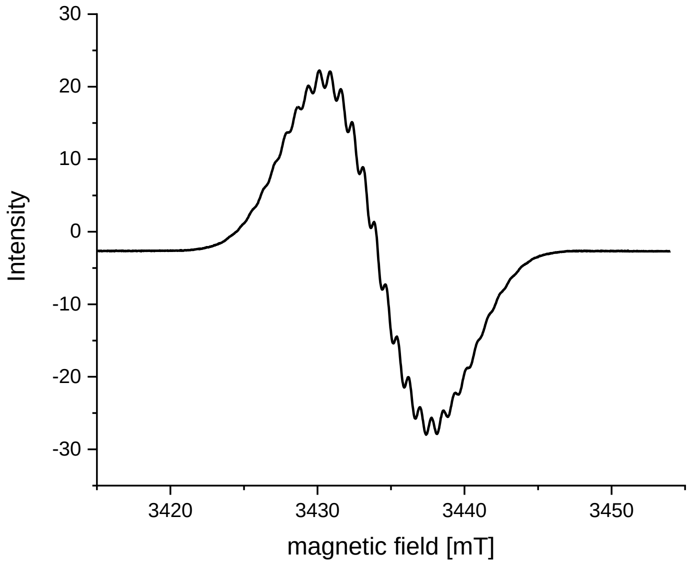

Compound 5c (C_3F_7-TAPP-Cl_4)

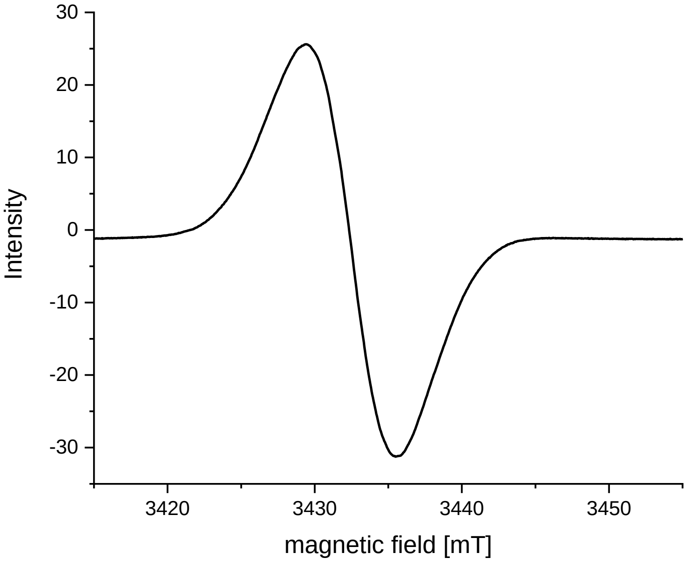

^{1}H and ^{19}F-NMR-Spectra of 5a^{2-}

^{1}H-NMR (600.13 MHz, $CDCl_3$, 295 K):

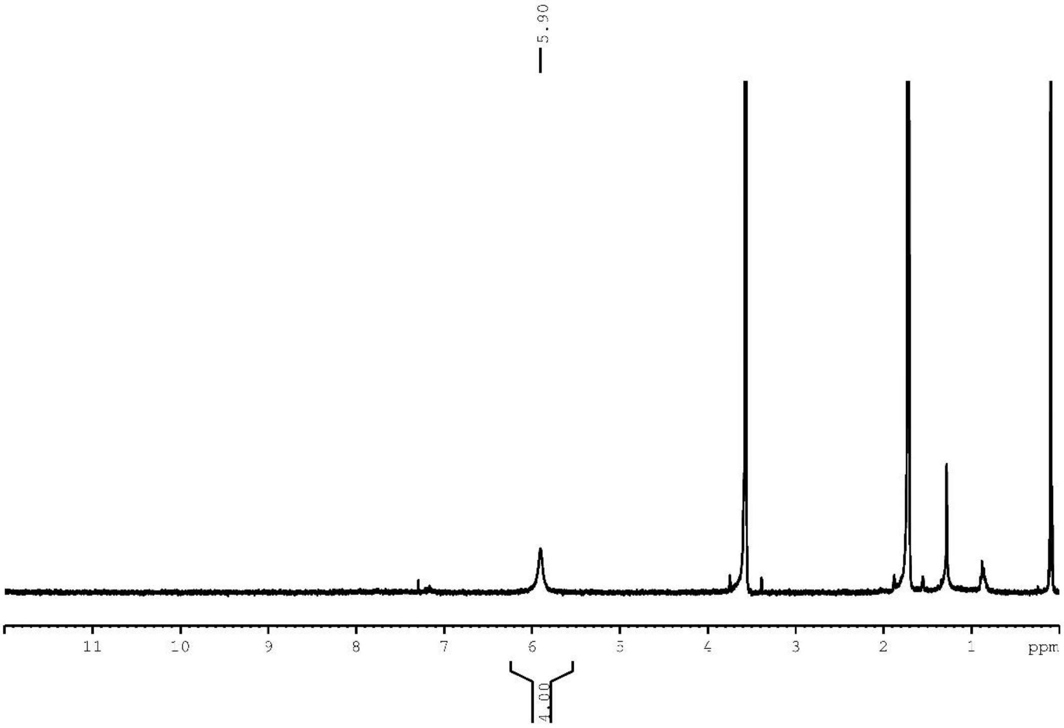

^{19}F-NMR (376.27 MHz, $CDCl_3$, 295 K):

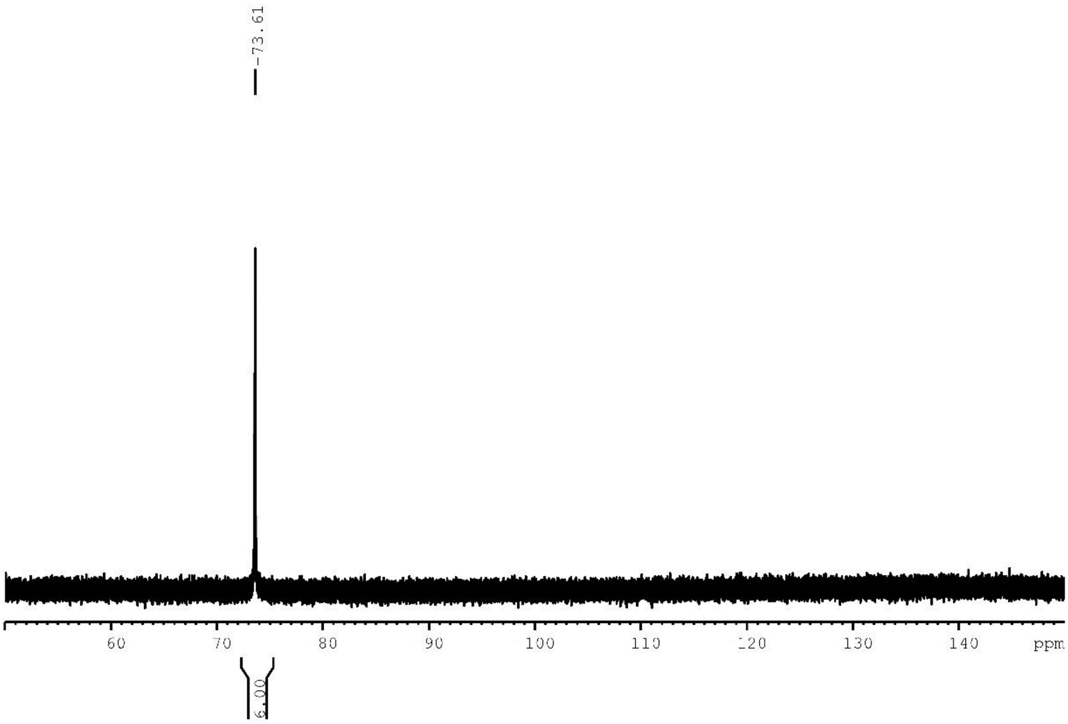

Absorption Spectra of 5a, $5a^{\cdot-}$ and $5a^{2-}$

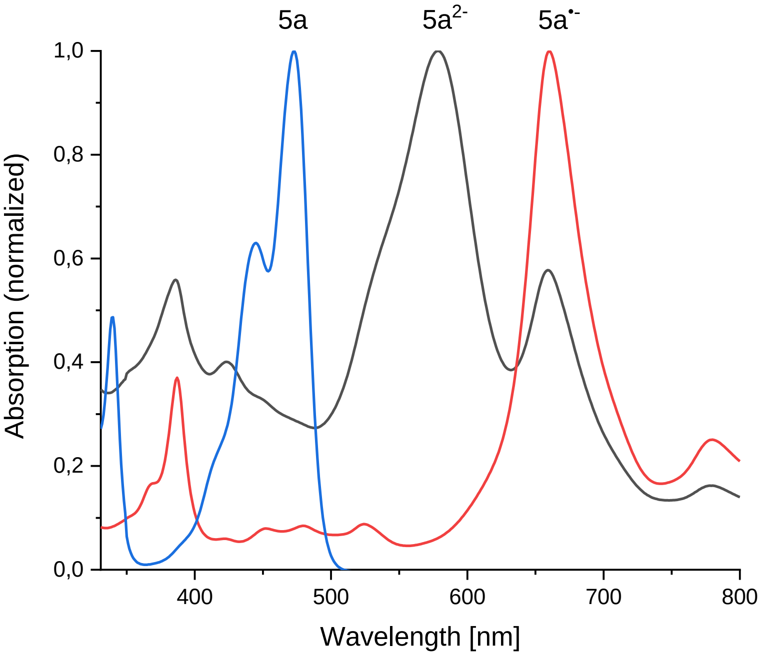

Computational Methods.

Coordinates of Compound 5a (CF_3-TAPP-Cl_4)

Atomic Type	Coordinates [Å] X	Y	Z
F	12.325717	9.972215	6.177854
F	13.588718	8.208711	6.170118
N	11.89735	8.918009	3.207875
N	14.141972	9.459602	3.822909
C	12.186645	9.130178	1.91354
C	11.165018	9.049499	0.912535
C	11.494489	9.164018	-0.41096
C	12.871626	9.303096	-0.85857
C	13.829384	9.691001	0.135888
C	13.491172	9.519844	1.508627
C	14.451716	9.700803	2.537211
C	15.787661	10.050507	2.162364
C	16.108134	10.270184	0.848039
C	13.364626	9.096085	-2.179707
C	12.895941	9.069868	4.072941
C	12.567808	8.809554	5.547253
N	16.462514	10.563853	-5.644494
N	14.810772	8.908884	-6.136989
C	16.045259	10.621293	-4.367938
C	16.618368	11.557203	-3.444644
C	16.250379	11.531307	-2.124735
C	15.329997	10.538514	-1.591405
C	14.545158	9.820819	-2.553905
C	14.969652	9.811005	-3.913503
C	14.353416	8.968602	-4.874803
C	13.292703	8.107799	-4.448847
C	12.837731	8.157526	-3.157837
C	15.119398	10.211612	-0.218041
C	15.833642	9.701257	-6.439323
F	11.488708	8.037425	5.681085
C	16.408267	9.52699	-7.851186
F	16.937587	10.6582	-8.322384
F	17.38503	8.601376	-7.822347
F	15.475452	9.110546	-8.712182
H	17.302691	12.316996	-3.823912
H	16.555587	10.062573	2.936529

H	10.127213	8.944265	1.230793
H	12.906861	7.370179	-5.153032
Cl	16.738785	12.870873	-1.124545
Cl	17.80613	10.382171	0.467317
Cl	10.19415	9.366004	-1.55294
Cl	11.758487	6.88322	-2.661287

Final Single Point Energy	-3575.65818245572 E_h	
HOMO:	-0.251282 E_h	-6.8377 eV
LUMO:	-0.151553 E_h	-4.1240 eV

Coordinates of Compound 5a$^-$ (CF_3-TAPP-Cl_4)

Atomic Type	Coordinates [Å]		
	X	Y	Z
F	12.236489	10.115348	6.164239
F	13.510945	8.363829	6.241052
N	11.8498	9.006571	3.232876
N	14.11934	9.46584	3.861496
C	12.161484	9.178881	1.922636
C	11.169929	9.099639	0.912183
C	11.538419	9.151013	-0.422133
C	12.897744	9.253329	-0.85034
C	13.848978	9.634751	0.156176
C	13.493116	9.498913	1.528235
C	14.459969	9.659011	2.561441
C	15.796098	9.944011	2.187018
C	16.118943	10.152312	0.855719
C	13.419335	9.017389	-2.182262
C	12.853959	9.14051	4.090182
C	12.502238	8.934787	5.563334
N	16.425544	10.625297	-5.681588
N	14.822485	8.909136	-6.174183
C	16.035868	10.640114	-4.380644
C	16.597932	11.551197	-3.449124
C	16.252095	11.471513	-2.109063
C	15.363956	10.48019	-1.588928
C	14.589384	9.759497	-2.560835
C	14.998457	9.774568	-3.924799
C	14.392983	8.915764	-4.886351
C	13.38365	8.022951	-4.448614
C	12.934445	8.073015	-3.139444
C	15.151449	10.128495	-0.196665
C	15.796793	9.759262	-6.467909

F	11.424213	8.156754	5.724418
C	16.328575	9.664793	-7.898639
F	16.759131	10.843958	-8.368205
F	17.378832	8.816289	-7.950386
F	15.404004	9.207504	-8.755676
H	17.278672	12.323913	-3.806141
H	16.567692	9.94965	2.95678
H	10.123021	9.008743	1.201982
H	12.99695	7.2789	-5.144699
Cl	16.818868	12.776868	-1.082291
Cl	17.834528	10.254543	0.494289
Cl	10.229049	9.25842	-1.587874
Cl	11.856553	6.776198	-2.653904

Final Single Point Energy -3575.77676843521E_h

Coordinates of Compound 5b (C_2F_5-TAPP-Cl_4)

	Coordinates [Å]		
Atomic Type	X	Y	Z
F	11.030829	9.984415	5.686548
F	13.129135	9.821167	6.304988
N	11.662435	9.195141	3.133142
N	13.89638	9.715321	3.80474
C	12.021131	9.247384	1.841344
C	11.046679	9.078395	0.805351
C	11.43825	9.056276	-0.505927
C	12.83594	9.142476	-0.899614
C	13.758935	9.592682	0.101584
C	13.355911	9.556499	1.466059
C	14.275649	9.804664	2.516875
C	15.640528	10.062994	2.176739
C	16.022769	10.162302	0.863934
C	13.375333	8.845315	-2.182752
C	12.622078	9.419424	4.028668
C	12.185414	9.306999	5.493563
N	16.477503	10.219751	-5.669335
N	14.813059	8.565598	-6.126668
C	16.081217	10.282682	-4.386194
C	16.671768	11.225114	-3.484027
C	16.293252	11.245924	-2.166933
C	15.342048	10.294577	-1.614904

C	14.570687	9.54239	-2.561114
C	15.0047	9.485268	-3.91511
C	14.3789	8.628463	-4.85849
C	13.326564	7.768187	-4.409546
C	12.866554	7.860057	-3.123757
C	15.075219	10.054499	-0.233457
C	15.829042	9.360912	-6.448631
C	16.277065	9.28166	-7.911076
F	17.552207	9.69687	-8.042862
F	16.195382	8.006767	-8.34806
H	17.370407	11.962018	-3.881687
H	16.374849	10.115697	2.981022
H	9.993665	9.022096	1.083058
H	12.947767	7.0064	-5.091651
Cl	16.806122	12.608056	-1.211899
Cl	17.73578	10.188579	0.543742
Cl	10.191746	9.14802	-1.720127
Cl	11.801711	6.596426	-2.575294
C	15.403035	10.152003	-8.854824
F	15.483995	11.436069	-8.490016
F	15.818521	10.035548	-10.114956
F	14.124431	9.774573	-8.792667
C	11.952871	7.841344	5.951135
F	10.985214	7.261689	5.241895
F	13.079427	7.136706	5.785167
F	11.610645	7.811771	7.239203

Final Single Point Energy -4051.28055243311 E_h
HOMO: -0.252173 E_h -6.8620 eV
LUMO: -0.152585 E_h -4.1520 eV

Coordinates of Compound $5b^-$ (C_2F_5-TAPP-Cl_4)

	Coordinates [Å]		
Atomic Type	X	Y	Z
F	10.866074	10.455061	5.334804
F	12.910057	10.565927	6.0978
N	11.639126	9.157245	3.104613
N	13.87201	9.694759	3.796664
C	12.054543	9.004859	1.819423
C	11.142071	8.691203	0.783073
C	11.584096	8.556018	-0.524864
C	12.955777	8.692177	-0.907867
C	13.84489	9.186778	0.107999

C	13.41239	9.244834	1.464285
C	14.315555	9.566779	2.519049
C	15.688316	9.712419	2.196815
C	16.084801	9.742918	0.870083
C	13.527613	8.45551	-2.222619
C	12.570662	9.516863	3.979425
C	12.048856	9.793085	5.39634
N	16.34541	10.379216	-5.718843
N	14.787974	8.636953	-6.261911
C	16.017068	10.287683	-4.404069
C	16.596033	11.152788	-3.442959
C	16.283214	11.006081	-2.101175
C	15.411874	9.986151	-1.60756
C	14.656422	9.264959	-2.593348
C	15.030909	9.35648	-3.965244
C	14.426626	8.529453	-4.956237
C	13.499548	7.546007	-4.525553
C	13.100143	7.502479	-3.199085
C	15.162937	9.65549	-0.21834
C	15.713809	9.546973	-6.536912
C	16.115869	9.665969	-8.013419
F	17.427936	9.98557	-8.126322
F	15.911909	8.497373	-8.667389
H	17.254977	11.952765	-3.779707
H	16.416734	9.799536	3.002845
H	10.082487	8.605104	1.022583
H	13.140552	6.806662	-5.241445
Cl	16.869649	12.271256	-1.037266
Cl	17.814292	9.731229	0.568642
Cl	10.3197	8.399176	-1.732247
Cl	12.185738	6.085083	-2.714991
C	15.335308	10.74327	-8.808457
F	15.569812	11.966588	-8.327556
F	15.705566	10.731618	-10.097437
F	14.021404	10.50536	-8.753282
C	11.80627	8.52904	6.258023
F	10.882172	7.73606	5.71481
F	12.938049	7.82756	6.394544
F	11.385523	8.8808	7.481461

Final Single Point Energy -4051.39883207785 E_h

Coordinates of Compound 5c (C_3F_7-TAPP-Cl_4)

Atomic Type	Coordinates [Å]		
	X	Y	Z
F	11.838829	10.242876	5.781019
N	11.937649	8.864832	3.14129
N	14.170651	9.392075	3.796202
C	12.28791	8.921428	1.848353
C	11.300677	8.771459	0.82212
C	11.673456	8.771993	-0.494466
C	13.065503	8.861915	-0.906471
C	14.008145	9.273538	0.093608
C	13.622296	9.220964	1.462737
C	14.551702	9.463391	2.506289
C	15.919353	9.692584	2.156345
C	16.288824	9.787642	0.83886
C	13.575098	8.622292	-2.212825
C	12.899959	9.092351	4.030784
C	12.437317	9.060091	5.487912
N	16.462605	10.310272	-5.737336
N	14.821318	8.645055	-6.22581
C	16.156381	10.244498	-4.428588
C	16.804463	11.101723	-3.483086
C	16.501314	11.013038	-2.148218
C	15.563386	10.03362	-1.623528
C	14.756384	9.344377	-2.588289
C	15.121724	9.39205	-3.963088
C	14.458448	8.597853	-4.935602
C	13.444345	7.685589	-4.498162
C	13.038431	7.688946	-3.191291
C	15.324474	9.728813	-0.24816
C	15.782249	9.507878	-6.547356
F	11.5098	8.089093	5.628893
C	16.197488	9.509884	-8.026105
F	17.171213	10.417255	-8.237223
F	16.684208	8.279481	-8.324668
H	17.488889	11.864837	-3.85493
H	16.663102	9.721106	2.953334
H	10.251358	8.717817	1.113745
H	13.0454	6.964291	-5.211875
Cl	17.098625	12.281881	-1.11674
Cl	17.995005	9.749284	0.489051
Cl	10.40746	8.895288	-1.684798
Cl	12.012477	6.381118	-2.673032
C	13.509942	8.771828	6.591325
F	12.820293	8.657008	7.745695
F	14.09012	7.583331	6.327191

C	15.07672	9.794371	-9.076633
F	15.598525	9.588952	-10.30348
F	14.05722	8.936986	-8.905962
C	14.646907	9.829416	6.842353
F	14.249484	11.056376	6.502101
F	14.953125	9.832375	8.14307
F	15.75438	9.531264	6.170338
C	14.502561	11.23879	-9.059352
F	14.130343	11.577939	-7.815367
F	15.406269	12.11576	-9.489762
F	13.430496	11.302983	-9.846612

Final Single Point Energy -4526.88967085511 E_h
HOMO: -0.253877 E_h -6.9084 eV
LUMO: -0.154487 E_h -4.2038 eV

Coordinates of Compound 5c$^-$ (C_3F_7-TAPP-Cl_4)

Atomic Type	Coordinates [Å]		
	X	Y	Z
F	11.542008	9.849499	5.758376
N	11.95362	8.817532	3.171292
N	14.227504	9.169702	3.841412
C	12.312162	8.864737	1.863864
C	11.341469	8.780272	0.835724
C	11.736835	8.755245	-0.491091
C	13.10748	8.774967	-0.895556
C	14.063152	9.122613	0.119219
C	13.672701	9.070813	1.4892
C	14.623114	9.22803	2.538309
C	15.985243	9.378825	2.181434
C	16.34786	9.500048	0.84712
C	13.623445	8.531986	-2.227274
C	12.933829	8.967763	4.051575
C	12.466192	8.885943	5.50364
N	16.467448	10.337031	-5.750261
N	14.812119	8.684097	-6.275455
C	16.184456	10.219418	-4.425329
C	16.849983	11.013452	-3.45946
C	16.570447	10.851773	-2.110323

C	15.640847	9.885283	-1.61175
C	14.812673	9.246904	-2.59839
C	15.157195	9.340852	-3.977289
C	14.475406	8.573717	-4.966265
C	13.48109	7.658516	-4.537561
C	13.087021	7.643418	-3.210434
C	15.400363	9.524603	-0.222891
C	15.76253	9.565399	-6.564519
F	11.855207	7.687651	5.711843
C	16.140606	9.635124	-8.050577
F	17.099201	10.565346	-8.26496
F	16.643724	8.430256	-8.431954
H	17.551157	11.77668	-3.796334
H	16.743125	9.364372	2.96466
H	10.285841	8.765336	1.106448
H	13.048112	6.965876	-5.258983
Cl	17.281163	12.047092	-1.041262
Cl	18.06906	9.439548	0.509448
Cl	10.453414	8.886453	-1.68123
Cl	11.9998	6.349425	-2.741814
C	13.539107	8.981468	6.633438
F	12.85147	8.886339	7.798729
F	14.366316	7.923571	6.565316
C	14.999038	9.949788	-9.069353
F	15.499923	9.788811	-10.319468
F	13.975683	9.093333	-8.927757
C	14.402109	10.296015	6.724365
F	13.856007	11.294945	6.027387
F	14.470762	10.690913	8.005351
F	15.645777	10.095346	6.304116
C	14.424988	11.39294	-9.012874
F	14.050635	11.717851	-7.772698
F	15.323443	12.282867	-9.439016
F	13.350441	11.472074	-9.806339

Final Single Point Energy -4527.01117312327E_h

Coordinates of Compound 5d (H-TAPP-Cl$_4$)

Atomic Type	Coordinates [Å]		
	X	Y	Z
N	11.839425	9.102857	3.210117
N	14.082235	9.651397	3.845876
C	12.177842	9.179289	1.912358
C	11.186042	9.019376	0.890981

C	11.543419	9.04734	-0.430053
C	12.925859	9.181145	-0.85903
C	13.867608	9.593683	0.141385
C	13.499645	9.510477	1.514481
C	14.436916	9.751287	2.55295
C	15.797209	10.013186	2.186638
C	16.146077	10.146226	0.869398
C	13.429483	8.981177	-2.177116
C	12.810503	9.334376	4.095546
N	16.347157	10.724039	-5.663865
N	14.70876	9.058904	-6.193731
C	16.007404	10.660312	-4.365421
C	16.623573	11.530947	-3.408329
C	16.306265	11.429339	-2.080266
C	15.388396	10.423088	-1.572832
C	14.593938	9.732796	-2.546885
C	14.971173	9.798028	-3.918445
C	14.328058	9.006014	-4.905652
C	13.318699	8.081168	-4.479479
C	12.910699	8.057238	-3.172633
C	15.16888	10.086538	-0.205141
C	15.686715	9.915649	-6.494827
H	17.294904	12.310084	-3.770551
H	16.551739	10.03762	2.973653
H	10.141208	8.935262	1.191523
H	12.931401	7.362139	-5.201995
Cl	16.855879	12.707472	-1.029034
Cl	17.850633	10.154263	0.493314
Cl	10.254514	9.155001	-1.601849
Cl	11.910924	6.715409	-2.678602
H	15.988571	9.958973	-7.549045
H	12.528546	9.253682	5.153174

Final Single Point Energy	- 2901.49261065712 E_h	
HOMO:	-0.236111 E_h	-6.4249 eV
LUMO:	-0.136157 E_h	-3.7050 eV

Coordinates of Compound 5d^{-} (H-TAPP-Cl$_4$)

	Coordinates [Å]		
Atomic Type	X	Y	Z
N	11.811966	9.159417	3.236398
N	14.080059	9.631735	3.877327
C	12.15499	9.227465	1.924782
C	11.180784	9.086064	0.902874
C	11.563619	9.079163	-0.427803

C	12.925019	9.182373	-0.849488
C	13.866744	9.584624	0.158733
C	13.494954	9.510754	1.532389
C	14.447018	9.715734	2.572299
C	15.797885	9.940498	2.198849
C	16.135691	10.089608	0.864272
C	13.448712	8.95971	-2.183795
C	12.797061	9.359849	4.110404
N	16.321498	10.768306	-5.698452
N	14.723278	9.050392	-6.222978
C	15.984603	10.699618	-4.385236
C	16.576737	11.565906	-3.429229
C	16.268976	11.430387	-2.085944
C	15.388284	10.424279	-1.582103
C	14.603052	9.726764	-2.562405
C	14.974559	9.79969	-3.936129
C	14.34926	8.979321	-4.91939
C	13.375309	8.042673	-4.481945
C	12.96466	8.034171	-3.159506
C	15.175331	10.061105	-0.193546
C	15.673215	9.938337	-6.513966
H	17.243723	12.355254	-3.775749
H	16.56283	9.959255	2.97539
H	10.13073	9.009173	1.18542
H	12.983856	7.315307	-5.193254
Cl	16.873692	12.696331	-1.026492
Cl	17.857539	10.129804	0.503709
Cl	10.255801	9.123529	-1.604529
Cl	11.939489	6.687034	-2.682432
H	15.969102	9.991744	-7.572954
H	12.510269	9.290408	5.171091
N	11.811966	9.159417	3.236398
N	14.080059	9.631735	3.877327
C	12.15499	9.227465	1.924782
C	11.180784	9.086064	0.902874
C	11.563619	9.079163	-0.427803
C	12.925019	9.182373	-0.849488

Final Single Point Energy -2901.59306515177 E_h

TFT Fabrication Process

The TFTs were fabricated in the bottom-gate, top-contact (inverted staggered) device architecture on heavily doped silicon substrates that also serve as a global gate electrode for all TFTs on the substrate. The gate dielectric is a stack of silicon dioxide (SiO_2) with a thickness of 100 nm grown by thermal oxidation in dry oxygen and aluminum oxide (Al_2O_3) with a thickness of 8 nm deposited by atomic layer deposition (Savannah 100, Cambridge NanoTech Inc.) at a substrate temperature of 250 °C. The Al_2O_3 surface was activated by oxygen plasma (Oxford Instruments) and then passivated with a self-assembled monolayer (SAM) by immersing the substrate into a 1-mM solution of n-tetradecylphosphonic acid (PCI Synthesis, Newburyport, MA, U.S.A.) in 2-propanol (VLSI grade) for one to two hours. The substrates were then rinsed in 2-propanol and dried on a hotplate at a temperature of 150 °C for 1 min. The resulting SiO_2/Al_2O_3/SAM gate dielectric has a total thickness of 110 nm and a unit-area capacitance of 34 nF/cm^2.[S1] The organic semiconductors were deposited onto the gate dielectric by sublimation in vacuum (Leybold UNIVEX 300) with a background pressure of about 10^{-6} mbar, at a substrate temperature of 70 °C, with a deposition rate of about 1 nm/min and with a nominal thickness of 30 nm. Finally, gold source and drain contacts were deposited onto the organic semiconductor layer by thermal evaporation in vacuum (Leybold UNIVEX 300) and patterned using a polyimide shadow mask. The TFTs have a channel length of 100 µm and a channel width of 200 µm. The current-voltage characteristics of the TFTs were measured in ambient air at room temperature.

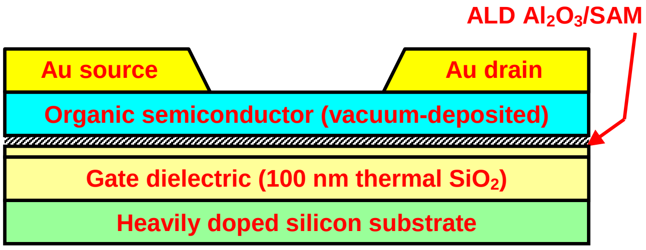

Crystal Structures of Compounds 5a-d

X-ray Crystal Structure Determinations

Crystal data and details of the structure determinations are compiled in Table S1. Full shells of intensity data were collected at low temperature with a Bruker AXS Smart 1000 CCD diffractometer (Mo-K_α radiation, sealed X-ray tube, graphite monochromator; compound **5b**) or an Agilent Technologies Supernova-E CCD diffractometer (Cu-K_α radiation, microfocus X-ray tube, multilayer mirror optics; compounds **5a** and **5c**·$CHCl_3$). Detector frames (typically ω-, occasionally φ-scans, scan width 0.4...1°) were integrated by profile fitting.[S2-S4] Data were corrected for air and detector absorption, Lorentz and polarization effects[S3,S4] and scaled essentially by application of appropriate spherical harmonic functions.[S5-S7] Absorption by the crystal was treated with a semiempirical multiscan method (as part of the scaling process), and augmented by a spherical correction,[S5-S7] or numerically (Gaussian grid).[S6,S7] For datasets collected with the microfocus tube an illumination correction was performed as part of the numerical absorption correction.[S8] The structures were solved by the heavy atom method combined with structure expansion by direct methods applied to difference structure factors (compound **5a**)[S9] or by the charge flip procedure (compounds **5b** and **5c**·$CHCl_3$)[S10] and refined by full-matrix least squares methods based on F^2 against all unique reflections.[S11] All non-hydrogen atoms were given anisotropic displacement parameters. Hydrogen atoms on the peropyrene core were fully refined with isotropic displacement parameters. The chloroform hydrogen in **5c**·$CHCl_3$ was refined riding.[S12]

CCDC 1908780 - 1908782 contains the supplementary crystallographic data for this paper. These data can be obtained free of charge from the Cambridge Crystallographic Data Centre's and FIZ Karlsruhe’s joint Access Service via https://www.ccdc.cam.ac.uk/structures/?.

Crystals of compounds **5a** and **5c** were grown by slow evaporation of saturated solutions of the compounds in $CHCl_3$. Crystals of **5b** were be grown by slow evaporation of a toluene solution.

Compound 5a (CF_3-TAPP-Cl_4)

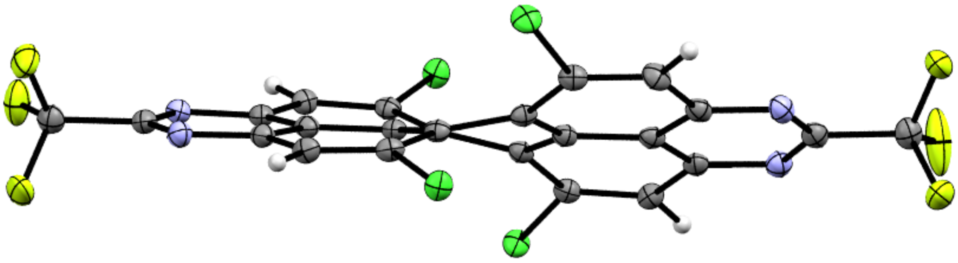

Ortep view (50% probability level) of 2 (C = grey ,N = blue, F = yellow, Cl = green, H = white).

Compound 5b (C_2F_5-TAPP-Cl_4)

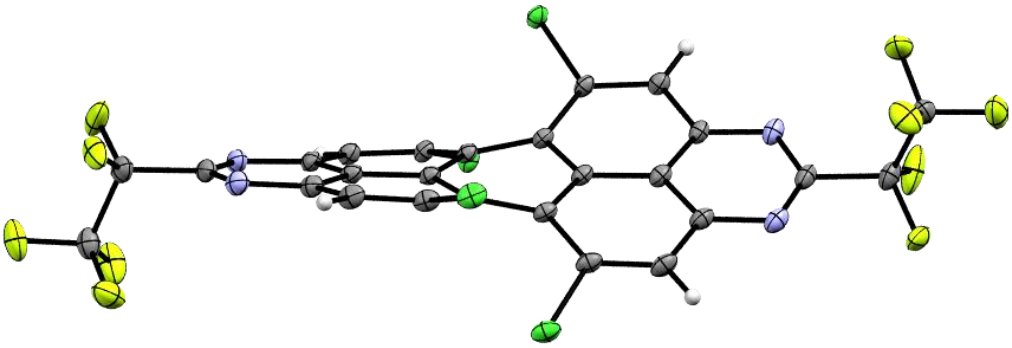

Ortep view (50% probability level) of 2 (C = grey ,N = blue, F = yellow, Cl = green, H = white).

Compound 5c (C_3F_7-TAPP-Cl_4)

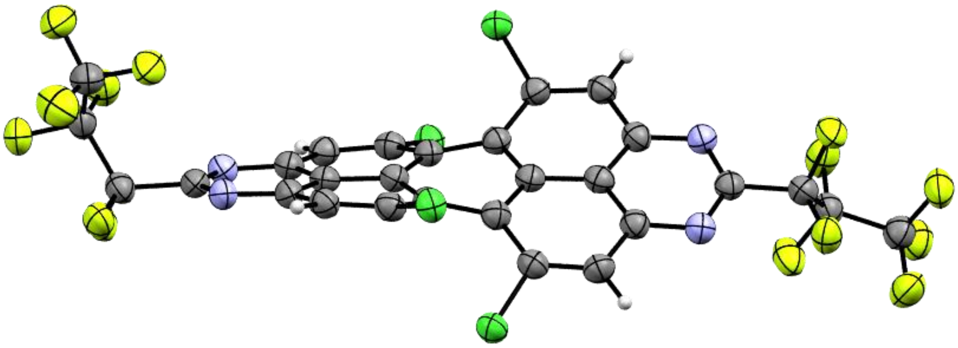

Ortep view (50% probability level) of 2 (C = grey ,N = blue, F = yellow, Cl = green, H = white).

Table S1. Details of the crystal structure determinations of compounds **5a**, **5b** and **5c**$\cdot CHCl_3$.

	5a	**5b**	**5c**$\cdot CHCl_3$
formula	$C_{24}H_4Cl_4F_6N_4$	$C_{26}H_4Cl_4F_{10}N_4$	$C_{29}H_5Cl_7F_{14}N_4$
crystal system	orthorhombic	monoclinic	triclinic
space group	*P bca*	*I* 2/*a*	*P* -1
a /Å	15.09084(13)	12.532(6) [b]	9.8735(4)
b /Å	12.56233(15)	13.358(6) [b]	12.5112(3)
c /Å	22.1683(2)	15.002(6) [b]	13.9911(6)
α /°			67.809(3)
β /°		98.345(11) [b]	83.349(4)
γ /°			78.762(3)
V /Å^3	4202.59(7)	2484.7(19) [b]	1567.91(11)
Z	8	4	2
M_r	604.11	704.13	923.52
F_{000}	2384	1384	904
d_c /Mgm^{-3}	1.910	1.882	1.956
μ /mm^{-1}	5.863	0.581	6.882
max., min. transmission factors	1.000, 0.598 [a]	0.7464, 0.6615 [c]	1.000, 0.8232 [c]
X-radiation, λ /Å	Cu-K_α, 1.54184	Mo-$K\alpha$, 0.71073	Cu-K_α, 1.54184
data collect. temperat. /K	120(1)	100(1)	120(1)
θ range /°	4.0 to 70.5	2.1 to 32.5	3.4 to 71.2
index ranges h,k,l	±18, ±15, ±26	±18, ±19, -21 ... 22	±12, ±15, -17 ... 16
reflections measured	130039	31427	52291
unique [R_{int}]	4000 [0.0649]	4283 [0.0298]	6004 [0.0500]
observed ($I \geq 2\sigma(I)$)	3508	3813	4793
data / restraints /parameters	4000 / 0 / 359	4283 / 0 / 207	6004 / 0 / 503
GooF on F^2	1.062	1.046	1.033
R indices ($F>4\sigma(F)$) $R(F)$, $wR(F^2)$	0.0305, 0.0748	0.0334, 0.0914	0.0504, 0.1338
R indices (all data) $R(F)$, $wR(F^2)$	0.0370, 0.0776	0.0384, 0.0965	0.0650, 0.1447
largest residual peaks /eÅ^{-3}	0.651, -0.250	0.677, -0.305	0.568, -0.434
CCDC deposition number	1908780	1908781	1908782

[a] numerical absorption correction; [b] includes systematic error contributions from Monte Carlo simulations; [c]

References

S1 R. Hofmockel, U. Zschieschang, U. Kraft, R. Rödel, N. H. Hansen, M. Stolte, F. Würthner, K. Takimiya, K. Kern, J. Pflaum, H. Klauk, *Org. Electron.*, **2013**, *14*, 3213-3221

S2 K. Kabsch, in: M. G. Rossmann, E. Arnold (eds.), *“International Tables for Crystallography” Vol. F*, Ch. 11.3, Kluwer Academic Publishers, Dordrecht, The Netherlands, **2001**.

S3 *SAINT*, Bruker AXS GmbH, Karlsruhe, Germany **1997-2017**.

S4 *CrysAlisPro*, Agilent Technologies UK Ltd., Oxford, UK **2011-2014** and Rigaku Oxford Diffraction, Rigaku Polska Sp.z o.o., Wrocław, Poland **2015-2019**.

S5 R. H. Blessing, *Acta Cryst.* **1995**, *A51*, 33.

S6 (a) G. M. Sheldrick, *SADABS*, Bruker AXS GmbH, Karlsruhe, Germany **2004-2014**; (b) L. Krause, R. Herbst-Irmer, G. M. Sheldrick, D. Stalke, *J. Appl. Cryst.* **2015**, *48*, 3.

S7 *SCALE3 ABSPACK*, *CrysAlisPro*, Agilent Technologies UK Ltd., Oxford, UK **2011-2014** and Rigaku Oxford Diffraction, Rigaku Polska Sp.z o.o., Wrocław, Poland **2015-2019**.

S8 W. R. Busing, H. A. Levy, *Acta Cryst.* **1957**, *10*, 180.

S9 (a) P. T. Beurskens, G. Beurskens, R. de Gelder, J. M. M. Smits, S. Garcia-Granda, R. O. Gould, *DIRDIF-2008*, Radboud University Nijmegen, The Netherlands, **2008**; (b) P. T. Beurskens, in: G. M. Sheldrick, C. Krüger, R. Goddard (eds.), *Crystallographic Computing 3*, Clarendon Press, Oxford, UK, **1985**, p. 216.

S10 (a) L. Palatinus, *SUPERFLIP*, EPF Lausanne, Switzerland and Fyzikální ústav AV ČR, v. v. i., Prague, Czech Republic, **2007-2014**; (b) L. Palatinus, G. Chapuis, *J. Appl. Cryst.* **2007**, 40, 786.

S11 (a) G. M. Sheldrick, *SHELXL-20xx*, University of Göttingen and Bruker AXS GmbH, Karlsruhe, Germany **2012-2018**; (b) W. Robinson, G. M. Sheldrick in: N. W. Isaaks, M. R. Taylor (eds.) „*Crystallographic Computing 4*“, Ch. 22, IUCr and Oxford University Press, Oxford, UK, **1988**; (c) G. M. Sheldrick, *Acta Cryst.* **2008**, *A64*, 112; (d) G. M. Sheldrick, *Acta Cryst.* **2015**, *C71*, 3.

S12 (a) J. S. Rollett in: F. R. Ahmed, S. R. Hall, C. P. Huber (eds.) „*Crystallographic Computing*“ p. 167, Munksgaard, Copenhagen, Denmark, **1970**; (b) D. Watkin in: N. W. Isaaks, M. R. Taylor (eds.) „*Crystallographic Computing 4*“, Ch. 8, IUCr and Oxford University Press, Oxford, UK, **1988**; (c) P. Müller, R. Herbst-Irmer, A. L. Spek, T. R. Schneider, M. R. Sawaya in: P. Müller (ed.) *“Crystal Structure Refinement”*, Ch. 5, Oxford University Press, Oxford, UK, **2006**; (d) D. Watkin, *J. Appl. Cryst.* **2008**, *41*, 491.